Available online at www.sciencedirect.com
ScienceDirect
Applied Mathematical Modelling 00 (2025) 1–30
Applied Mathematical Modelling

A port-Hamiltonian framework for the modeling and FEM discretization of hyperelastic systems

Cristobal Ponce[a,*], Yongxin Wu[b], Yann Le Gorrec[b], Hector Ramirez[a]

[a] *Departamento de Electrónica, Universidad Técnica Federico Santa María, Valparaíso, Chile.*
[b] *Université Marie et Louis Pasteur, Supmicrotech, Institut FEMTO-ST, Besançon, France.*

Abstract

This article presents a systematic modeling methodology for deriving the infinite-dimensional port-Hamiltonian representation of geometrically nonlinear and hyperelastic systems, and a structure-preserving mixed FEM approach. The proposed methods provide a rigorous framework for obtaining the dynamic nonlinear partial differential equations governing these systems, ensuring that they are consistent with a Stokes–Dirac geometric structure. This structure is fundamental for modular multiphysics modeling and nonlinear passivity-based control. The modeling methodology is rooted in a total Lagrangian formulation, incorporating Green–Lagrange strains and second Piola–Kirchhoff stresses, where generalized displacements and strains define the interconnection structure. Using the generalized Hamilton's principle, infinite-dimensional port-Hamiltonian systems are systematically derived. To preserve the structure upon spatial discretization, a three-field mixed finite element approach is proposed, in which displacements, strains, and stresses are explicitly treated as independent variables to retain the port-Hamiltonian structure. The effectiveness of the framework is demonstrated through model derivation and simulations, using a geometrically nonlinear planar beam with Saint Venant–Kirchhoff material, and a compressible nonlinear 2D elasticity problem with a Neo-Hookean material model, as illustrative examples.

Keywords: Port-Hamiltonian systems, Modeling, Structure-preserving discretization, Nonlinear elastodynamics, Hyperelasticity.

1. Introduction

Multiphysics models are central to emerging applications such as hybrid nanofluids in electro-magneto-hydrodynamics, memory response of nano-piezoelectric plates, and rotor dynamics control using mechatronic bearings [1–3]. These applications involve strong couplings between mechanical, thermal, electromagnetic, and fluidic subsystems, where the flexible mechanical component is often a key component. Nonlinear mechanical systems undergoing large deformations are fundamental in engineering applications ranging from aerospace structures to soft robotics and advanced materials. Accurate modeling of these systems is essential for predicting their dynamic behavior, optimizing designs, and developing effective control strategies [4–7].

*Corresponding author
Email addresses: cristobal.ponces@usm.cl (Cristobal Ponce), yongxin.wu@femto-st.fr (Yongxin Wu), legorrec@femto-st.fr (Yann Le Gorrec), hector.ramireze@usm.cl (Hector Ramirez)

Classical modeling approaches based on continuum mechanics, particularly those using Lagrangian formulations, have been extensively developed to describe such systems [8–10]. However, the inherent geometric and material nonlinearities due to large deformations and hyperelastic behavior pose significant challenges for both numerical simulation and control design [7, 11–13]. Moreover, Lagrangian and classical Hamiltonian systems are intrinsically *closed*, meaning they do not account for interactions with the environment through well-defined input and output ports [14]. This structural limitation makes them less suitable for modular modeling in multiphysics applications and may complicate their use in control design. Therefore, many existing control strategies rely on simplified or approximate models, which often compromise essential structural properties such as energy conservation and passivity. These simplifications frequently overlook the complexities introduced by large deformations and nonlinear material responses, which are critical for accurately capturing the system dynamics. As a result, conventional approaches may fail to fully represent the underlying physics, limiting their applicability in real-world scenarios.

Port-Hamiltonian Systems (PHS) offer a structured framework for modeling and controlling nonlinear physical systems while preserving key physical properties such as passivity, energy conservation, and interconnection structure [14, 15]. Unlike classical Hamiltonian formulations, PHS are intrinsically *open* systems, as they explicitly capture energy exchange with the environment through power-conjugated ports. By centering the modeling process on energy flows, this formalism naturally supports modular design and the coherent interconnection of subsystems across different physical domains. These features make PHS particularly well-suited for multiphysics modeling and nonlinear control design [16, 17]. They have been successfully exploited in passivity-based control (PBC) strategies, which leverage the inherent stability of passive systems to develop robust controllers in electrical, fluid, thermodynamic, and mechanical applications [18–22]. For a comprehensive review of the PHS framework, the reader is referred to [23, 24].

The modeling of geometrically nonlinear mechanical systems within the PHS framework has largely been pursued through case-specific formulations. Several contributions have addressed models using von Kármán strains assumptions, including Euler–Bernoulli and Timoshenko beams [25–28], with extensions to two-dimensional plate models [29]. A more general three-dimensional formulation employing the Green–Lagrange strain tensor and the second Piola–Kirchhoff stress tensor was proposed in [30]. Additionally, geometrically exact models have been developed, such as the beam formulation introduced in [31]. In parallel, the treatment of hyperelastic systems has gained increasing attention. Examples include one-dimensional formulations using the right Cauchy–Green deformation tensor and a Neo–Hookean material law for strings [32], as well as incompressible von Kármán beam models incorporating Neo–Hookean and Mooney–Rivlin constitutive laws [33]. Regarding spatial discretization, conventional techniques, such as standard finite element, finite differences, and finite volume methods, generally fail to preserve the PHS structure, often leading to a loss of passivity and degraded numerical stability [34], which are critical properties for nonlinear control applications. To address these limitations, structure-preserving discretization methods have been the subject of extensive research [34–40]. Within the finite element family, most structure-preserving approaches for elastodynamics rely on mixed formulations. Some are based on the Hellinger–Reissner variational principle [39], which involves inverting the constitutive law, an assumption that is not applicable for general nonlinear hyperelastic materials. In such cases, it is well established that weakly enforcing the constitutive relation and treating strain and stress as independent fields yields a mimetic discretization and avoids the need to invert the constitutive law [41]. To the best of our knowledge, there is currently no general and systematic methodology for modeling and discretizing geometrically nonlinear and hyperelastic mechanical systems within the PHS framework. As discussed, existing works are restricted to specific geometries and assume simplified kinematics and material behaviors. Furthermore, structure-preserving discretizations are typically introduced in an ad hoc fashion, without a clear connection to the variational methods used to derive the continuous models. This lack of generality and systematic formulation hinders the extension of port-Hamiltonian modeling and structure-preserving discretization of systems involving large deformations and hyperelastic constitutive laws.

In this work, we address these gaps by proposing a unified total Lagrangian framework for modeling and discretizing multidimensional, geometrically nonlinear, and hyperelastic port-Hamiltonian systems. Analogous to the classical treatment of Lagrangian systems, where continuous models and their finite element discretizations are derived from Hamiltons principle, our approach enables the direct and systematic

derivation of PHS models and their structure-preserving discretizations based on the generalized Hamiltons principle [42]. Specifically, this work makes two main contributions: (i) a systematic modeling methodology for directly deriving the port-Hamiltonian representation of geometrically nonlinear and hyperelastic systems, including explicit definitions of energy and co-energy variables, the nonlinear skew-adjoint differential operator, and power-conjugated boundary inputs and outputs; and (ii) a specialized three-field-based structure-preserving mixed finite element discretization approach. A key feature of the methodology is the modular modeling and the decoupling of the interconnection structure from the constitutive laws. The kinematic relations are encoded in the nonlinear differential operator defining the interconnection structure, whereas the constitutive law is captured entirely through the co-energy variables. Consequently, the model's state variables comprise momentum, Green–Lagrange strains, and displacements, while the co-energy variables include velocity, second Piola–Kirchhoff stresses, and body forces. Lastly, this separation enables modularity and flexibility, allowing the substitution of different strain measures, such as infinitesimal or von Kármán strains, or various hyperelastic material models, while preserving the underlying PHS structure.

The paper is organized as follows. Section 2 reviews the generalized Hamilton's principle, the governing equations of nonlinear elastodynamics, and the infinite-dimensional PHS framework. Section 3 introduces the proposed modeling methodology, and Section 4 presents the structure-preserving spatial discretization. Section 5 demonstrates the effectiveness of the framework through numerical examples. Finally, Section 6 provides conclusions and discusses future directions.

2. Background

In this section, we present the fundamental equations of elastodynamics, focusing on their derivation from the Generalized Hamilton's Principle (GHP) [42]. This principle extends the classical Hamilton's principle by treating displacements, stresses, and strains as independent variables and can be interpreted as a dynamic counterpart of the Hu–Washizu principle. Additionally, we introduce the port-Hamiltonian formalism in the context of Stokes–Dirac structures. For simplicity, spatial and temporal dependencies will often be omitted.

2.1. Nonlinear elastodynamics

Let $\mathcal{B}_0 \subset \mathbb{R}^3$ be the volume of an elastic body in the reference configuration, as in Fig. 1. The motion of a hyperelastic solid undergoing large deformations is described by the displacement field $\mathbf{u}(\mathbf{X}, t) \in \mathbb{R}^3$, defined as:

$$\mathbf{u}(\mathbf{X}, t) = \mathbf{x}(\mathbf{X}, t) - \mathbf{X}, \tag{1}$$

which assigns to each point $\mathbf{X} \in \mathcal{B}_0$ a displacement vector specifying its current position $\mathbf{x}(\mathbf{X}, t)$ at time $t > t_0$ in the deformed configuration, relative to the reference configuration. The deformation gradient tensor $\underline{\mathbf{F}} \in \mathbb{R}^{3\times3}$, which characterizes local deformations, is given by:

$$\underline{\mathbf{F}} = \frac{\partial \mathbf{x}}{\partial \mathbf{X}} = \underline{\mathbf{I}} + \nabla \mathbf{u}, \tag{2}$$

where $\underline{\mathbf{I}} \in \mathbb{R}^{3\times3}$ is the second-order identity tensor, and $\nabla(\cdot)$ represents the gradient operator with respect to the material coordinates $\mathbf{X}$. The Green–Lagrange strain tensor $\underline{\mathbf{E}} \in \mathbb{R}^{3\times3}$, which measures nonlinear strain in the reference configuration, is defined as:

$$\underline{\mathbf{E}} = \frac{1}{2}\left(\underline{\mathbf{F}}^\top \underline{\mathbf{F}} - \underline{\mathbf{I}}\right) = \frac{1}{2}\left(\nabla \mathbf{u} + (\nabla \mathbf{u})^\top + (\nabla \mathbf{u})^\top \nabla \mathbf{u}\right). \tag{3}$$

The second Piola–Kirchhoff stress tensor $\underline{\mathbf{T}} \in \mathbb{R}^{3\times3}$, which represents stresses energy-conjugated to $\underline{\mathbf{E}}$, is related to the strain energy density function $W(\underline{\mathbf{E}}) \in \mathbb{R}$ by:

$$\underline{\mathbf{T}} = \frac{\partial W}{\partial \underline{\mathbf{E}}}, \tag{4}$$

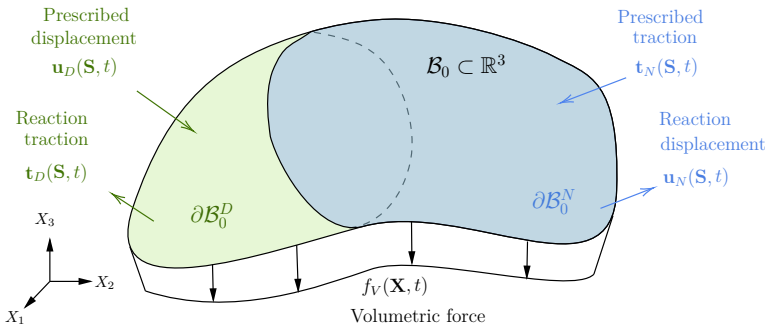

Figure 1: Three-dimensional body and external work.

where $W(\underline{\mathbf{E}})$ represents the deformation energy per unit reference volume $\mathcal{B}_0$. Therefore, the elastic energy $\mathcal{U} \in \mathbb{R}$ is defined as:

$$\mathcal{U} = \int_{\mathcal{B}_0} W(\underline{\mathbf{E}})\, d\mathbf{X}. \tag{5}$$

Remark 1. In material Cartesian coordinates $\mathbf{X} = \{X_1, X_2, X_3\} \in \mathcal{B}_0$, the displacement field $\mathbf{u}(\mathbf{X},t)$ is expressed component-wise as:

$$u_i(\mathbf{X},t) = x_i(\mathbf{X},t) - X_i, \tag{6}$$

where $i = \{1,2,3\}$, X_i are the material coordinates in the reference configuration, and x_i are the spatial coordinates in the deformed configuration. The components of the deformation gradient $\underline{\mathbf{F}}$ are given by:

$$F_{ij} = \frac{\partial x_i}{\partial X_j} = \delta_{ij} + \frac{\partial u_i}{\partial X_j}, \tag{7}$$

where δ_{ij} is the Kronecker delta, defined as $\delta_{ij} = 1$ if $i = j$, and $\delta_{ij} = 0$ otherwise. Finally, the components of the Green–Lagrange strain tensor $\underline{\mathbf{E}}$ are given by:

$$E_{ij} = \frac{1}{2}\left(\frac{\partial u_i}{\partial X_j} + \frac{\partial u_j}{\partial X_i} + \sum_{k=1}^{3} \frac{\partial u_k}{\partial X_i}\frac{\partial u_k}{\partial X_j}\right), \tag{8}$$

where the summation over k is written explicitly.

Before stating the GHP, let us first consider the continuum body in Fig. 1, with reference volume $\mathcal{B}_0 \subset \mathbb{R}^3$ and boundary surface $\partial\mathcal{B}_0 = \partial\mathcal{B}_0^D \cup \partial\mathcal{B}_0^N$, where $\partial\mathcal{B}_0^D$ and $\partial\mathcal{B}_0^N$ denote the portions of the boundary on which Dirichlet and Neumann boundary conditions (BC) are applied, respectively. In Fig. 1, external work is performed on the body through both its volume and boundary. A distributed volumetric force $f_V(\mathbf{X},t) \in \mathbb{R}^3$ acts on $\mathcal{B}_0$, which represents self-weight and external inputs. On $\partial\mathcal{B}_0^D$, the prescribed displacement $\mathbf{u}_D(\mathbf{S},t) \in \mathbb{R}^3$ induces its energy-conjugated reaction traction $\mathbf{t}_D(\mathbf{S},t) \in \mathbb{R}^3$. Conversely, on $\partial\mathcal{B}_0^N$, the prescribed traction $\mathbf{t}_N(\mathbf{S},t) \in \mathbb{R}^3$ induces its energy-conjugated reaction displacement $\mathbf{u}_N(\mathbf{S},t) \in \mathbb{R}^3$. The variable $\mathbf{S} \in \partial\mathcal{B}_0$ denotes a curvilinear coordinate along the boundary.

Definition 1 (GHP, [42]). The GHP states that the true evolution of $\mathbf{u}(\mathbf{X},t)$ between two specific times t_1 and t_2 is a stationary point of the generalized action functional under admissible independent variations $\delta\mathbf{u}$, $\delta\underline{\mathbf{E}}$, $\delta\underline{\mathbf{T}}$ and $\delta\mathbf{t}_D$, i.e.:

$$\int_{t_1}^{t_2} \delta\left(\mathcal{T} - \mathcal{U}_E + \mathcal{W}_E\right) dt = 0, \tag{9}$$

$$\delta\mathbf{u}(\mathbf{S},t) = 0 \; on \; \partial\mathcal{B}_0^D \; for \; all \; t, \tag{10}$$

$$\delta\mathbf{u}(\mathbf{X},t_1) = \delta\mathbf{u}(\mathbf{X},t_2) = 0 \; for \; all \; \mathbf{X}, \tag{11}$$

where δ is the variational operator, $\mathcal{T} \in \mathbb{R}$ is the kinetic energy, $\mathcal{U}_E \in \mathbb{R}$ is the extended elastic energy, and $\mathcal{W}_E \in \mathbb{R}$ is the extended external work, respectively defined as:

$$\mathcal{T} = \frac{1}{2}\int_{\mathcal{B}_0} \rho_0\, \dot{\mathbf{u}} \cdot \dot{\mathbf{u}}\, d\mathbf{X}, \tag{12}$$

$$\mathcal{U}_E = \int_{\mathcal{B}_0} [\, \underline{\mathbf{T}} : (\, \underline{\mathbf{E}}(\mathbf{u}) - \underline{\mathbf{E}}\,) + W(\underline{\mathbf{E}}\,)\,]\, d\mathbf{X}, \tag{13}$$

$$\mathcal{W}_E = \int_{\mathcal{B}_0} f_V \cdot \mathbf{u}\, d\mathbf{X} + \int_{\partial\mathcal{B}_0^N} \mathbf{t}_N \cdot \mathbf{u}\, d\mathbf{S} + \int_{\partial\mathcal{B}_0^D} \mathbf{t}_D \cdot (\, \mathbf{u} - \mathbf{u}_D\,)\, d\mathbf{S}, \tag{14}$$

where $\rho_0(\mathbf{X}) \in \mathbb{R}$ is the density of the material, and $\underline{\mathbf{E}}(\mathbf{u})$ denotes the Green–Lagrange strain tensor expressed in terms of $\mathbf{u}(\mathbf{X}, t)$. Consequently, its variation must be expressed in terms of $\delta\mathbf{u}$.

Remark 2. The GHP shares conceptual similarities with the Hu–Washizu principle, as both formulate variational frameworks that treat displacements, strains, and stresses as independent variables. However, the Hu–Washizu principle was originally developed for elastostatics, enforcing homogeneous Dirichlet boundary conditions strongly by restricting the admissible displacement fields. In contrast, the GHP is introduced as a dynamic extension and explicitly incorporates tractions on Dirichlet boundaries as independent variables, enabling the weak imposition of non-homogeneous Dirichlet boundary conditions. This feature makes the GHP particularly well suited for dynamic problems and boundary control scenarios.

Applying the GHP from Definition 1 yields:

$$\text{for all } \mathbf{X} \in \mathcal{B}_0 : \quad \begin{cases} \rho_0 \ddot{\mathbf{u}} = & \mathrm{Div}(\underline{\mathbf{F}}\,\underline{\mathbf{T}}) + f_V, \\ \underline{\mathbf{E}} = & \underline{\mathbf{E}}(\mathbf{u}), \\ \underline{\mathbf{T}} = & \frac{\partial W}{\partial \underline{\mathbf{E}}}, \end{cases} \tag{15}$$

$$\text{for all } \mathbf{S} \in \partial\mathcal{B}_0^D : \quad \mathbf{u}_D = \mathbf{u}, \tag{16}$$

$$\text{for all } \mathbf{S} \in \partial\mathcal{B}_0^N : \quad \mathbf{t}_N = \underline{\mathbf{F}}\,\underline{\mathbf{T}}\,\hat{\mathbf{N}}, \tag{17}$$

where $\underline{\mathbf{F}}$ is expressed in terms of $\mathbf{u}(\mathbf{X}, t)$, i.e., $\underline{\mathbf{F}}(\mathbf{u})$, and $\hat{\mathbf{N}} \in \mathbb{R}^3$ is the outward unit vector normal to $\partial\mathcal{B}_0$. From (15), the first equation represents the kinetic equation (balance of linear momentum), the second describes kinematics (strain-displacement relation), and the third defines the constitutive law for a hyperelastic solid (stress-strain relation). Dirichlet and Neumann BC follow from (16) and (17), respectively.

2.2. Port-Hamiltonian systems

Let $\Omega \subset \mathbb{R}^\ell$ with $\ell = \{1, 2, 3\}$ be an open set representing an ℓ-dimensional spatial domain and $\partial\Omega$ its boundary, such that $\mathtt{X} \in \Omega$ and $\mathtt{S} \in \partial\Omega$. A conservative dynamic system is an infinite-dimensional PHS if it is expressed as [14]:

$$\begin{aligned} \text{for } \mathtt{X} \in \Omega: \quad \dot{x}(\mathtt{X}, t) &= \mathcal{J}(x)\delta_x H(x) + \mathcal{G}(x) u_d(\mathtt{X}, t) \\ y_d(\mathtt{X}, t) &= \mathcal{G}(x)^* \delta_x H(x), \\ \text{for } \mathtt{S} \in \partial\Omega: \quad u_\partial(\mathtt{S}, t) &= \mathcal{B}_\partial\, \delta_x H(x), \\ y_\partial(\mathtt{S}, t) &= \mathcal{C}_\partial\, \delta_x H(x), \end{aligned} \tag{18}$$

where $x(\mathtt{X}, t)$ is the state, $u_d(\mathtt{X}, t)$, $y_d(\mathtt{X}, t)$ are the distributed input and output ports, respectively. $\mathcal{J}(x) = -\mathcal{J}(x)^*$ is a formal skew-adjoint differential operator, $\mathcal{G}(x)$, $\mathcal{G}(x)^*$ are the input mapping operator and its formal adjoint, respectively. The variational derivative of the Hamiltonian functional $H(x)$ with respect to $x(\mathtt{X}, t)$, denoted by $\delta_x H(x)$, defines the co-energy variables. The boundary operators $\mathcal{B}_\partial$ and $\mathcal{C}_\partial$ provide the boundary input $u_\partial(\mathtt{S}, t)$ and output $y_\partial(\mathtt{S}, t)$ ports [43, 44]. To ensure that an infinite-dimensional PHS is defined within the Stokes–Dirac structure, the operators $\mathcal{J}(x)$, $\mathcal{B}_\partial$, and $\mathcal{C}_\partial$ must satisfy the Stokes' theorem; see [45, Assumption 1] for further details.

Definition 2 (Stokes–Dirac structure, [44]). Let $\mathscr{F}_d$, $\mathscr{E}_d$, and $\mathscr{B}_d$ be Hilbert spaces, where $\mathscr{F}_d$ is the flow space, its dual $\mathscr{E}_d$ is the effort space, and $\mathscr{B}_d = \mathscr{F}_d \times \mathscr{E}_d$ is called the bond space of power variables. A Stokes–Dirac structure on $\mathscr{B}_d$ is a subspace $\mathscr{D}_s \subset \mathscr{B}_d$ such that $\mathscr{D}_s = \mathscr{D}_s^{\perp}$ with respect to a bilinear form $\langle\langle \cdot, \cdot \rangle\rangle$ given by:

$$\langle\langle (\mathtt{f}_1, \mathtt{f}_{\partial_1}, \mathtt{e}_1, \mathtt{e}_{\partial_1}), (\mathtt{f}_2, \mathtt{f}_{\partial_2}, \mathtt{e}_2, \mathtt{e}_{\partial_2}) \rangle\rangle = \langle \mathtt{e}_1 | \mathtt{f}_2 \rangle_{in}^{\Omega} + \langle \mathtt{e}_2 | \mathtt{f}_1 \rangle_{in}^{\Omega} + \langle \mathtt{e}_{\partial_1} | \mathtt{f}_{\partial_2} \rangle_{in}^{\partial\Omega} + \langle \mathtt{e}_{\partial_2} | \mathtt{f}_{\partial_1} \rangle_{in}^{\partial\Omega}, \tag{19}$$

where $\langle \cdot | \cdot \rangle_{in}^{\Omega}$ and $\langle \cdot | \cdot \rangle_{in}^{\partial\Omega}$ are inner products defined over the spatial domain Ω and its boundary $\partial\Omega$, respectively. Therefore, for any $(\mathtt{f}, \mathtt{f}_\partial, \mathtt{e}, \mathtt{e}_\partial) \in \mathscr{D}_s$ it holds that $\langle\langle (\mathtt{f}, \mathtt{f}_\partial, \mathtt{e}, \mathtt{e}_\partial), (\mathtt{f}, \mathtt{f}_\partial, \mathtt{e}, \mathtt{e}_\partial) \rangle\rangle = 0$, which can be generally verified by applying the Stokes theorem.

Considering the infinite-dimensional PHS in (18), let $\mathtt{f} = [\mathtt{f}_s, \mathtt{f}_e, \mathtt{f}_\partial]^\top$ and $\mathtt{e} = [\mathtt{e}_s, \mathtt{e}_e, \mathtt{e}_\partial]^\top$, where $\mathtt{f}_s = \dot{x}$, $\mathtt{f}_e = u_d$, $\mathtt{f}_\partial = u_\partial$, $\mathtt{e}_s = \delta_x H$, $\mathtt{e}_e = -y_d$, $\mathtt{e}_\partial = -y_\partial$. Then the set:

$$\mathscr{D}_s = \{(\mathtt{f}, \mathtt{e}) \in \mathscr{B}_d \mid \mathtt{f}_s = \mathcal{J}\mathtt{e}_s + \mathcal{G}\mathtt{f}_e\,,\ \mathtt{e}_e = -\mathcal{G}^*\mathtt{e}_s,\ \mathtt{f}_\partial = \mathcal{B}_\partial \mathtt{e}_s,\ \mathtt{e}_\partial = -\mathcal{C}_\partial \mathtt{e}_s\} \tag{20}$$

is a Stokes–Dirac structure. With the above definitions of $\mathtt{f}$ and $\mathtt{e}$, it follows that system (18) is conservative, and that the energy exchange with the environment is characterized by:

$$\dot{H} = \langle y_d |\, u_d \rangle_{in}^{\Omega} + \langle y_\partial |\, u_\partial \rangle_{in}^{\partial\Omega}. \tag{21}$$

Remark 3. Infinite-dimensional PHS have been generalized to dissipative systems within Stokes–Dirac structures by partitioning the distributed ports into open and resistive ports. For additional details, see [14, 46]. In addition, infinite-dimensional PHS can also be defined in jet-bundle structures of variational complexes, often called port-Lagrangian systems (PLS) [47]. This approach, based on differential geometry, uses jet bundles to describe field interactions and higher-order spatial derivatives, offering a powerful tool for modeling and analyzing complex systems. For details on PHS in jet bundles, see [48, 49], and for a comparison with PHS in Stokes–Dirac structures, see [50].

In elastodynamics, the differential operator arises from the kinematic equation. In the geometrically nonlinear setting, displacements and strains are related through a first-order differential operator without cross derivatives, as shown in (3). Hence, this work focuses on systems defined by this class of operators.

Definition 3 (Differential operators, [33]). Let $\mathtt{X}$=$\{X_1, \ldots, X_\ell\}$ be a set of orthogonal coordinate axes, $\Omega \subset \mathbb{R}^\ell$ an open set, $v(\mathtt{X}) \in \mathbb{R}^m$ and $w(\mathtt{X}) \in \mathbb{R}^n$ two vector-valued functions. The first-order differential operator $\mathcal{F}_\mathtt{X}$ and its formal adjoint $\mathcal{F}_\mathtt{X}^*$ are given by:

$$\begin{aligned} \mathcal{F}_\mathtt{X}\, w(\mathtt{X}) &= F_0(\mathtt{X})\, w(\mathtt{X}) + \textstyle\sum_{k=1}^{\ell} F_k(\mathtt{X})\, \partial_k w(\mathtt{X}), \\ \mathcal{F}_\mathtt{X}^* v(\mathtt{X}) &= F_0(\mathtt{X})^\top v(\mathtt{X}) - \textstyle\sum_{k=1}^{\ell} \partial_k (F_k(\mathtt{X})^\top v(\mathtt{X})), \end{aligned}$$

with $\partial_k = \partial/\partial X_k$ and $F_0(\mathtt{X})$, $F_k(\mathtt{X}) \in \mathbb{R}^{m\times n}$.

Remark 4. In Definition 3, a vector-valued function $v(\mathtt{X}) \in \mathbb{R}^m$ (and analogously $w(\mathtt{X}) \in \mathbb{R}^n$) is understood as a mapping that assigns a vector in the Euclidean space $\mathbb{R}^m$ to each point $\mathtt{X} \in \Omega$. In contrast, in differential geometry, a vector field $v(\mathtt{X})$ is formally interpreted as a first-order differential operator, i.e., a map assigning to each point a directional derivative of the form:

$$v(\mathtt{X}) = v_i(\mathtt{X}) \frac{\partial}{\partial \mathtt{X}_i}.$$

This distinction is important to avoid confusion regarding the notion of $v(\mathtt{X}) \in \mathbb{R}^m$ in Definition 3.

Lemma 1 (Integration by parts, [33]). Consider Definition 3. For any smooth functions $v(\mathtt{X}) \in \mathbb{R}^m$ and $w(\mathtt{X}) \in \mathbb{R}^n$ defined on the closure $\bar{\Omega} = \Omega \cup \partial\Omega$, the following identity holds:

$$\int_{\Omega} \left[v(\mathtt{X})^\top \mathcal{F}_{\mathtt{X}}\, w(\mathtt{X}) - w(\mathtt{X})^\top \mathcal{F}_{\mathtt{X}}^*\, v(\mathtt{X}) \right] d\mathtt{X} = \int_{\partial\Omega} w(\mathtt{S})^\top F_\partial(\mathtt{S})\, v(\mathtt{S})\, d\mathtt{S},$$

with $F_\partial(\mathtt{S}) \in \mathbb{R}^{n\times m}$ a boundary matrix function given by:

$$F_\partial(\mathtt{S}) = \textstyle\sum_{k=1}^{\ell} F_k(\mathtt{S})^\top\, \hat{n}_k(\mathtt{S}),$$

and $\hat{n}_k(\mathtt{S})$ is the k-th component of the outward unit vector $\hat{n}(\mathtt{S}) \in \mathbb{R}^\ell$ normal to $\partial\Omega$.

3. Modeling

This section addresses the modeling of a broad class of multidimensional systems. To ensure clarity and consistency throughout the presentation of results, a notation is established that effectively organizes and distinguishes the relevant elements.

Notation

Let $\mathbf{X} = \{X_1, X_2, X_3\} \in \mathcal{B}_0$ denote the material Cartesian coordinates of a three-dimensional body, as illustrated in Fig. 2. The reference volume is decomposed as $\mathcal{B}_0 = \Omega \times \Omega^c$, where $\Omega \subset \mathbb{R}^\ell$ is the ℓ-dimensional spatial domain over which the model parameters are distributed, and Ω^c is a complementary domain. The boundary surface is assumed to be $\partial\mathcal{B}_0 = \partial\Omega \times \Omega^c$, with $\partial\Omega = \partial\Omega_D \cup \partial\Omega_N$ denoting the Dirichlet and Neumann boundary portions, respectively. Let $\mathtt{X} \subseteq \mathbf{X}$ with $\mathtt{X} \in \Omega$ represent the subset of coordinates where the parameters are distributed, and let $\mathtt{X}^c \subset \mathbf{X}$ with $\mathtt{X}^c \in \Omega^c$ denote its complement. With this, a volume differential is given by $d\mathbf{X} = d\mathtt{X}^c\, d\mathtt{X}$, and the integral of an arbitrary separable function $g(\mathbf{X}) = g_1(\mathtt{X})g_2(\mathtt{X}^c)$ over $\mathcal{B}_0$ becomes:

$$\int_{\mathcal{B}_0} g(\mathbf{X})\, d\mathbf{X} = \int_{\Omega} g_1(\mathtt{X}) \int_{\Omega^c} g_2(\mathtt{X}^c)\, d\mathtt{X}^c\, d\mathtt{X}.$$

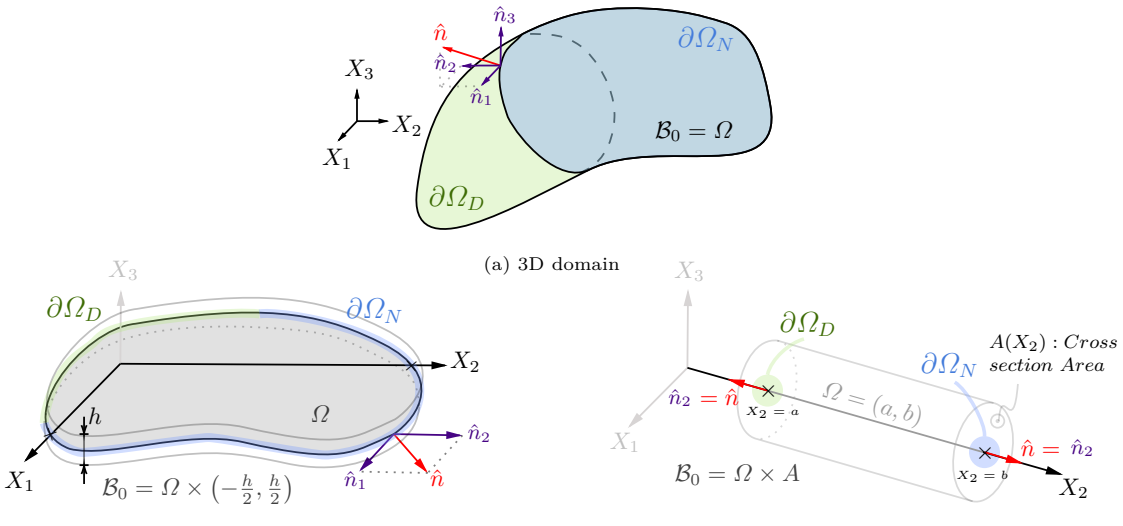

(a) 3D domain

(b) 2D domain

(c) 1D domain

Figure 2: Schemes to illustrate notation [51].

3.1. Considered class of systems

The class of systems considered in this study must satisfies the following assumptions, which serve as foundational pillars for characterizing the proposed modeling framework.

Assumption 1. Consider three-dimensional bodies with density $\rho_0(\mathtt{X}) \in \mathbb{R}$, whose kinematic assumptions yield a displacement field $\mathbf{u}(\mathbf{X}, t) \in \mathbb{R}^3$ as:

$$\mathbf{u}(\mathbf{X}, t) = \bar{M}_1(\mathtt{X}^c)\, r(\mathtt{X}, t), \tag{22}$$

where $\bar{M}_1(\mathtt{X}^c) \in \mathbb{R}^{3\times n}$ is a full-rank matrix, and $r(\mathtt{X}, t) = [r_1(\mathtt{X}, t) \cdots r_n(\mathtt{X}, t)]^\top \in \mathbb{R}^n$ denotes the vector of generalized displacements.

Let $\vec{E} = [E_{11}\ E_{22}\ E_{33}\ 2E_{12}\ 2E_{13}\ 2E_{23}]^\top \in \mathbb{R}^6$ be the Voigt-strain vector containing the six independent components of the Green–Lagrange strain tensor $\underline{\mathbf{E}}$. This vector may have up to six nonzero components, so we define $\boldsymbol{\varepsilon}(\mathbf{X}, t) \in \mathbb{R}^d$ as the vector composed of its nonzero entries, with $d \leq 6$.

Assumption 2. Assume that $\boldsymbol{\varepsilon}(\mathbf{X}, t) \in \mathbb{R}^d$, the nonzero components of $\vec{E}$, can be expressed as:

$$\boldsymbol{\varepsilon}(\mathbf{X}, t) = \bar{M}_2(\mathtt{X}^c)\, \epsilon(\mathtt{X}, t), \tag{23}$$

where $\bar{M}_2(\mathtt{X}^c) \in \mathbb{R}^{d\times m}$ is a full-rank matrix, and $\epsilon(\mathtt{X}, t) = [\epsilon_1(\mathtt{X}, t) \cdots \epsilon_m(\mathtt{X}, t)]^\top \in \mathbb{R}^m$ is defined as the vector of generalized strains. Furthermore, assume that the strain energy density function evaluated at $\boldsymbol{\varepsilon}(\mathbf{X}, t)$, denoted $W(\boldsymbol{\varepsilon}) \in \mathbb{R}$, is integrable over the complementary domain Ω^c, and defines:

$$\Psi(\epsilon) = \int_{\Omega^c} W(\underline{\mathbf{E}})\, d\mathtt{X}^c = \int_{\Omega^c} W\big(\bar{M}_2(\mathtt{X}^c)\, \epsilon(\mathtt{X}, t)\big)\, d\mathtt{X}^c, \tag{24}$$

where $\Psi(\epsilon) \in \mathbb{R}$ is referred to as the generalized strain energy density function.

The full-rank assumptions on $\bar{M}_1(\mathtt{X}^c)$ and $\bar{M}_2(\mathtt{X}^c)$ are required to ensure the invertibility of the mass density matrix and the positive definiteness of the stiffness density matrix, respectively, as discussed in [51] for linear systems. However, these conditions can often be relaxed when the complementary domain Ω^c is symmetric with respect to its centroidal coordinates, as such symmetry leads to equivalent properties. Furthermore, note from (24) that, due to the explicit dependence of the matrix $\bar{M}_2(\mathtt{X}^c)$ on $\mathtt{X}^c$, general strain energy functions $W(\underline{\mathbf{E}})$ may fail to satisfy the integrability condition. This issue arises, for example, when using Neo–Hookean or Mooney–Rivlin models for beams or plates. Nevertheless, it can be addressed by approximating the non-integrable terms via polynomial expansions. A detailed analysis of this strategy in the context of hyperelastic von Kármán beam models within the PHS framework is presented in [33]. Despite these limitations, the proposed assumptions still encompass a broad class of systems relevant to engineering applications. Examples of displacement fields $\mathbf{u}(\mathbf{X}, t)$ of the form (22) are provided in [52, Appendix B], while strain energy functions $W(\underline{\mathbf{E}})$ for hyperelastic materials are reviewed in [53–56].

3.2. Energy and external work

To derive the PHS representation for the considered class of systems, the GHP is applied. This first requires expressing the kinetic energy, elastic energy, and external work in terms of the generalized variables.

Proposition 1 (Kinetic energy, [51]). The generalized momentum $p(\mathtt{X}, t) \in \mathbb{R}^n$, the mass density matrix $\mathcal{M}(\mathtt{X}) = \mathcal{M}(\mathtt{X})^\top > 0 \in \mathbb{R}^{n\times n}$, the kinetic energy $T(p) \in \mathbb{R}$, and the co-energy variable $e_p(\mathtt{X}, t) \in \mathbb{R}^n$ are defined as:

$$p(\mathtt{X}, t) = \mathcal{M}(\mathtt{X})\, \dot{r}(\mathtt{X}, t), \tag{25}$$

$$\mathcal{M}(\mathtt{X}) = \rho_0(\mathtt{X}) \int_{\Omega^c} \bar{M}_1(\mathtt{X}^c)^\top \bar{M}_1(\mathtt{X}^c)\, d\mathtt{X}^c, \tag{26}$$

$$T(p) = \frac{1}{2} \int_{\Omega} p(\mathtt{X},t)^\top \mathcal{M}(\mathtt{X})^{-1} p(\mathtt{X},t)\, d\mathtt{X}, \tag{27}$$

$$e_p(\mathtt{X},t) = \mathcal{M}(\mathtt{X})^{-1} p(\mathtt{X},t). \tag{28}$$

Proof. According to Assumption 1, the displacement field implies $\dot{\mathbf{u}}(\mathbf{X},t) = \bar{M}_1(\mathtt{X}^c)\,\dot{r}(\mathtt{X},t)$. Then, from the definition in (12), we obtain:

$$\begin{aligned} \mathcal{T} &= \frac{1}{2} \int_{\mathcal{B}_0} \rho_0(\mathtt{X})\, \dot{\mathbf{u}}(\mathbf{X},t)^\top \dot{\mathbf{u}}(\mathbf{X},t)\, d\mathbf{X} \\ &= \frac{1}{2} \int_{\Omega} \dot{r}(\mathtt{X},t)^\top \mathcal{M}(\mathtt{X})\, \dot{r}(\mathtt{X},t)\, d\mathtt{X}, \end{aligned}$$

where the mass density matrix $\mathcal{M}(\mathtt{X})$ is given by (26). Since $\bar{M}_1(\mathtt{X}^c)$ is full-rank, or assuming that Ω^c is symmetric with respect to its centroidal coordinates, $\mathcal{M}(\mathtt{X})$ is invertible, and thus $\mathcal{T} = T(p)$. By definition, $e_p(\mathtt{X},t)$ is the variational derivative of $T(p)$ with respect to $p(\mathtt{X},t)$. □

Proposition 2 (Elastic energy). The time derivative of the generalized strains $\dot{\epsilon}(\mathtt{X},t) \in \mathbb{R}^m$, the elastic energy $U(\epsilon) \in \mathbb{R}$, and the co-energy variable $e_\epsilon(\mathtt{X},t) \in \mathbb{R}^m$ are defined as:

$$\dot{\epsilon}(\mathtt{X},t) = \mathcal{F}_{\mathtt{X}}(r)\, \dot{r}(\mathtt{X},t), \tag{29}$$

$$U(\epsilon) = \int_{\Omega} \Psi(\epsilon)\, d\mathtt{X}, \tag{30}$$

$$e_\epsilon(\mathtt{X},t) = \frac{\partial \Psi(\epsilon)}{\partial \epsilon}, \tag{31}$$

where $\mathcal{F}_{\mathtt{X}}(r)$ is a differential operator belonging to the same class as in Definition 3, with associated matrices $F_0(r)$, $F_k(r) \in \mathbb{R}^{m\times n}$.

Proof. The generalized strain $\epsilon(\mathtt{X},t)$ is a function of $r(\mathtt{X},t)$ and its spatial derivatives. Then, by applying the chain rule, $\dot{\epsilon}(\mathtt{X},t)$ can be written as in (29), where $\mathcal{F}_{\mathtt{X}}(r)$ is a differential operator modulated by $r(\mathtt{X},t)$ and its spatial derivatives. From the definition of elastic energy $\mathcal{U}$ in (5), and considering Assumption 2, we obtain $\mathcal{U} = U(\epsilon)$. By definition, $e_\epsilon(\mathtt{X},t)$ is the variational derivative of $U(\epsilon)$ with respect to $\epsilon(\mathtt{X},t)$, and is defined as the generalized stress. □

In the following, the extended external work $\mathcal{W}_E$, previously defined in (14), is reformulated to be applicable for any spatial domain $\Omega \subset \mathbb{R}^\ell$.

Proposition 3 (Extended external work). The extended external work $\mathcal{W}_E$ can be expressed as:

$$\mathcal{W}_E = \int_{\Omega} r(\mathtt{X},t)^\top \left[B_d\, u_d(\mathtt{X},t) + b(\mathtt{X})\right] d\mathtt{X} + \int_{\partial\Omega_N} r(\mathtt{S},t)^\top \tau_N(\mathtt{S},t)\, d\mathtt{S} + \int_{\partial\Omega_D} \left[r(\mathtt{S},t) - r_D(\mathtt{S},t)\right]^\top \tau_D(\mathtt{S},t)\, d\mathtt{S}, \tag{32}$$

where $B_d\, u_d(\mathtt{X},t) \in \mathbb{R}^n$ denotes the generalized distributed load, with B_d an algebraic input map and $u_d(\mathtt{X},t)$ the distributed input, $b(\mathtt{X}) \in \mathbb{R}^n$ is the generalized body force due to the self-weight, $\tau_N(\mathtt{S},t) \in \mathbb{R}^n$ is the imposed generalized traction on $\partial\Omega_N$, $\tau_D(\mathtt{S},t) \in \mathbb{R}^n$ is the generalized reaction traction on $\partial\Omega_D$, and $r_D(\mathtt{S},t) \in \mathbb{R}^n$ is the imposed generalized displacement on $\partial\Omega_D$.

Proof. The extended external work $\mathcal{W}_E$ defined in (14) is composed of the three terms:

$$\mathcal{W}_E = \underbrace{\int_{\mathcal{B}_0} f_V \cdot \mathbf{u}\, d\mathbf{X}}_{(a)} + \underbrace{\int_{\partial\mathcal{B}_0^N} \mathbf{t}_N \cdot \mathbf{u}\, d\mathbf{S}}_{(b)} + \underbrace{\int_{\partial\mathcal{B}_0^D} \mathbf{t}_D \cdot [\mathbf{u} - \mathbf{u}_D]\, d\mathbf{S}}_{(c)}.$$

According to Assumption 1, for (a) we have:

$$\begin{aligned}(a) &= \int_{\Omega} r(\mathtt{X},t)^{\top} \int_{\Omega^c} \bar{M}_1(\mathtt{X}^c)^{\top} f_V \, d\mathtt{X}^c \, d\mathtt{X} \\ &= \int_{\Omega} r(\mathtt{X},t)^{\top} f_{\Omega}(\mathtt{X},t) \, d\mathtt{X} \\ &= \int_{\Omega} r(\mathtt{X},t)^{\top} [B_d \, u_d(\mathtt{X},t) + b(\mathtt{X})] \, d\mathtt{X},\end{aligned}$$

where $f_{\Omega} := \int_{\Omega^c} \bar{M}_1^{\top} f_V \, d\mathtt{X}^c$ and the partition $f_{\Omega}(\mathtt{X},t) = B_d \, u_d(\mathtt{X},t) + b(\mathtt{X})$ is considered. For the terms (b) and (c) we obtain:

$$\begin{aligned}(b) &= \int_{\partial\Omega_N} r(\mathtt{S},t)^{\top} \int_{\Omega^c} \bar{M}_1(\mathtt{X}^c)^{\top} \mathbf{t}_N \, d\mathtt{X}^c \, d\mathtt{S} \\ &= \int_{\partial\Omega_N} r(\mathtt{S},t)^{\top} \tau_N(\mathtt{S},t) \, d\mathtt{S}, \\ (c) &= \int_{\partial\Omega_D} [r(\mathtt{S},t) - r_D(\mathtt{S},t)]^{\top} \int_{\Omega^c} \bar{M}_1(\mathtt{X}^c)^{\top} \mathbf{t}_D \, d\mathtt{X}^c d\mathtt{S} \\ &= \int_{\partial\Omega_D} [r(\mathtt{S},t) - r_D(\mathtt{S},t)]^{\top} \tau_D(\mathtt{S},t) \, d\mathtt{S}.\end{aligned}$$

Considering the above, $\mathcal{W}_E$ in (14) is equivalent to the expression in Proposition 3. □

The extended external work is associated with the external loads acting on the body, either distributed over the spatial domain $\Omega \subset \mathbb{R}^{\ell}$ or applied through its boundary $\partial\Omega$. The distributed loads comprise two components: $B_d \, u_d(\mathtt{X},t)$, representing the generalized distributed load with $u_d(\mathtt{X},t)$ as an external input, and $b(\mathtt{X})$, representing the body force due to self-weight. On $\partial\Omega_N$, $\tau_N(\mathtt{S},t)$ denotes the imposed generalized traction, with its power-conjugated reaction being the generalized velocity $v_N(\mathtt{S},t)$. Conversely, on $\partial\Omega_D$, $v_D(\mathtt{S},t) = \dot{r}_D(\mathtt{S},t)$ is the imposed generalized velocity, whose power-conjugated reaction is the generalized traction $\tau_D(\mathtt{S},t)$. For a visual representation of these variables, see Fig. 3.

Remark 5. Dissipative effects are not considered in the present formulation. The incorporation of phenomena such as viscous damping requires special attention, especially in nonlinear systems. While such effects can be introduced subsequently in either infinite-dimensional or finite-dimensional settings, they must be carefully examined on a case-by-case basis to ensure consistency of the formulation.

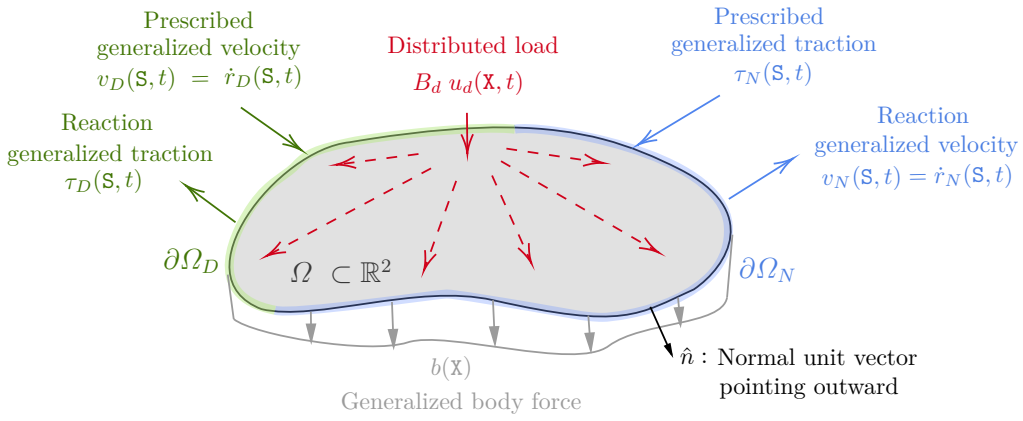

Figure 3: Scheme to illustrate the extended external work.

3.3. Systematic modeling methodology

The infinite-dimensional PHS representation for the considered class of hyperelastic systems is presented in the following theorem.

Theorem 1 (Infinite-dimensional PHS). Let $x(\mathtt{X},t) = [p(\mathtt{X},t)^\top \ \epsilon(\mathtt{X},t)^\top \ r(\mathtt{X},t)^\top]^\top \in \mathbb{R}^{2n+m}$ be the state variables, and $\delta_x H(x) = [e_p(\mathtt{X},t)^\top \ e_\epsilon(\mathtt{X},t)^\top - b(\mathtt{X})^\top]^\top \in \mathbb{R}^{2n+m}$ be the co-energy variables. From Propositions 1, 2 and 3, the dynamics of the geometrically nonlinear and hyperelastic systems in PHS form is given by:

$$\begin{aligned} \underbrace{\begin{bmatrix} \dot{p}(\mathtt{X},t) \\ \dot{\epsilon}(\mathtt{X},t) \\ \dot{r}(\mathtt{X},t) \end{bmatrix}}_{\dot{x}(\mathtt{X},t)} &= \underbrace{\begin{bmatrix} 0 & -\mathcal{F}_{\mathtt{X}}(r)^* & -1 \\ \mathcal{F}_{\mathtt{X}}(r) & 0 & 0 \\ 1 & 0 & 0 \end{bmatrix}}_{\mathcal{J}(x)=-\mathcal{J}(x)^*} \underbrace{\begin{bmatrix} e_p(\mathtt{X},t) \\ e_\epsilon(\mathtt{X},t) \\ -b(\mathtt{X}) \end{bmatrix}}_{\delta_x H(x)} + \underbrace{\begin{bmatrix} B_d \\ 0 \\ 0 \end{bmatrix}}_{\mathcal{G}} u_d(\mathtt{X},t) \\ y_d(\mathtt{X},t) &= \mathcal{G}^* \delta_x H(x) = B_d^\top e_p(\mathtt{X},t). \end{aligned} \tag{33}$$

The boundary inputs and outputs $u_\partial(\mathtt{S},t)$, $y_\partial(\mathtt{S},t) \in \mathbb{R}^{2n}$ are defined as:

$$\begin{aligned} u_\partial(\mathtt{S},t) &= \begin{bmatrix} \tau_N(\mathtt{S},t)^\top & v_D(\mathtt{S},t)^\top \end{bmatrix}^\top, \\ y_\partial(\mathtt{S},t) &= \begin{bmatrix} v_N(\mathtt{S},t)^\top & \tau_D(\mathtt{S},t)^\top \end{bmatrix}^\top, \end{aligned} \tag{34}$$

with

$$\begin{aligned} \tau_N(\mathtt{S},t) &= F_\partial(r) e_\epsilon(\mathtt{S},t), \quad v_N(\mathtt{S},t) = e_p(\mathtt{S},t) \qquad (\text{on } \partial\Omega_N), \\ \tau_D(\mathtt{S},t) &= F_\partial(r) e_\epsilon(\mathtt{S},t), \quad v_D(\mathtt{S},t) = e_p(\mathtt{S},t) \qquad (\text{on } \partial\Omega_D), \end{aligned} \tag{35}$$

where the matrix $F_\partial(r) \in \mathbb{R}^{n\times m}$ is defined by:

$$F_\partial(r) = \textstyle\sum_{k=1}^{\ell} F_k(r)^\top \hat{n}_k(\mathtt{S}), \tag{36}$$

with $\hat{n}_k(\mathtt{S})$ denoting the k-th component of the outward unit vector $\hat{n}(\mathtt{S}) \in \mathbb{R}^\ell$ normal to $\partial\Omega$. The total energy function, given by the Hamiltonian $H(x)$, is:

$$H(x) = \int_\Omega \left(\frac{1}{2} p(\mathtt{X},t)^\top \mathcal{M}(\mathtt{X})^{-1} p(\mathtt{X},t) + \Psi(\epsilon) - r(\mathtt{X},t)^\top b(\mathtt{X}) \right) d\mathtt{X}, \tag{37}$$

and the power balance satisfies:

$$\dot{H} = \int_\Omega u_d(\mathtt{X},t)^\top y_d(\mathtt{X},t)\, d\mathtt{X} + \int_{\partial\Omega} u_\partial(\mathtt{S},t)^\top y_\partial(\mathtt{S},t)\, d\mathtt{S}. \tag{38}$$

Proof. The result follows from the application of the GHP, with full details provided in Appendix A. □

The infinite-dimensional PHS models presented in Theorem 1 incorporate geometric nonlinearity through the differential operator $\mathcal{F}_{\mathtt{X}}(r)$, while material nonlinearity (hyperelasticity) appears exclusively in the generalized stress $e_\epsilon(\mathtt{X}.t)$. Moreover, [51, Theorem 1] on systematic modeling of linear systems is a particular case of Theorem 1, where the strain measure is the infinitesimal strain tensor and the strain energy density function corresponds to the Saint Venant-Kirchhoff model, which is equivalent to Hooke's law in the context of small deformation theory. We also remark that the system described in Theorem 1 defines a Stokes–Dirac structure $\mathscr{D}_s$ over the space $\mathscr{B}_d$ introduced in Definition 2. The Stokes–Dirac structure is given by:

$$\mathscr{D}_s = \left\{ (\mathtt{f}_\Omega, \mathtt{f}_\partial, \mathtt{e}_\Omega, \mathtt{e}_\partial) \in \mathscr{B}_d \;\middle|\; \underbrace{\begin{bmatrix} \mathtt{f}_s \\ \mathtt{e}_e \end{bmatrix}}_{\mathtt{f}_\Omega} = \underbrace{\begin{bmatrix} \mathcal{J} & \mathcal{G} \\ -\mathcal{G}^* & 0 \end{bmatrix}}_{\mathcal{J}_\Omega} \underbrace{\begin{bmatrix} \mathtt{e}_s \\ \mathtt{f}_e \end{bmatrix}}_{\mathtt{e}_\Omega}, \ \mathtt{f}_\partial = \mathcal{B}_\partial \mathtt{e}_s, \ \mathtt{e}_\partial = -\mathcal{C}_\partial \mathtt{e}_s \right\},$$

where the flow and effort variables are defined as $\mathtt{f}_s = \dot{x}$, $\mathtt{f}_e = u_d$, $\mathtt{f}_\partial = u_\partial$, $\mathtt{e}_s = \delta_x H$, $\mathtt{e}_e = -y_d$, $\mathtt{e}_\partial = -y_\partial$, and the boundary input and output operators as:

$$\mathcal{B}_\partial \mathtt{e}_s = \begin{bmatrix} F_\partial e_\epsilon\big|_{\partial\Omega_N} \\ e_p\big|_{\partial\Omega_D} \end{bmatrix}, \quad \mathcal{C}_\partial \mathtt{e}_s = \begin{bmatrix} e_p\big|_{\partial\Omega_N} \\ F_\partial e_\epsilon\big|_{\partial\Omega_D} \end{bmatrix}.$$

The Stokes–Dirac structure satisfies the condition $\mathscr{D}_s = \mathscr{D}_s^\perp$, where orthogonality is understood with respect to the bilinear pairing (19). The proof follows by showing both inclusions $\mathscr{D}_s \subset \mathscr{D}_s^\perp$ and $\mathscr{D}_s^\perp \subset \mathscr{D}_s$, as in [45, Proposition 2], to which we refer the reader for further details.

Now, a systematic procedure is proposed for modeling geometrically nonlinear and hyperelastic PHS over multidimensional spatial domains. This procedure involves defining the system's state variables, formulating the Hamiltonian function, constructing the nonlinear differential operator, and specifying the distributed and boundary ports. These steps provide a structured approach to accurately capturing the system's dynamics and energy exchanges.

Procedure: To derive a PHS representation for a flexible mechanical system with density $\rho_0(\mathtt{X})$, where kinematic assumptions lead to a displacement field $\mathbf{u}(\mathbf{X}, t)$ as in Assumption 1, and the constitutive behavior is governed by a hyperelastic model with a strain energy density function $W(\underline{\mathbf{E}})$ satisfying Assumption 2, follow the steps below:

Step 1. Calculate the mass density matrix $\mathcal{M}(\mathtt{X})$ and define the generalized momentum variables $p(\mathtt{X}, t)$, the co-energy variables $e_p(\mathtt{X}, t)$ and the kinetic energy $T(p)$. (Proposition 1).

Step 2. Identify the nonzero components of the Voigt-strain vector and define the generalized strain $\epsilon(\mathtt{X}, t)$. Then, compute its time derivative to construct the differential operator $\mathcal{F}_\mathtt{X}(r)$ and its formal adjoint $\mathcal{F}_\mathtt{X}(r)^*$. (Proposition 2).

Step 3. Compute the generalized strain energy density function $\Psi(\epsilon)$. Then, compute the co-energy variable $e_\epsilon(\mathtt{X}, t)$ and the elastic potential energy $U(\epsilon)$. (Proposition 2).

Step 4. If applicable, define the generalized distributed load $B_d\, u_d(\mathtt{X}, t)$ and the generalized body force $b(\mathtt{X})$. (Proposition 3).

Step 5. Apply Theorem 1 to obtain the infinite-dimensional nonlinear PHS representation, including the definitions of boundary inputs $u_\partial(\mathtt{S}, t)$ and boundary outputs $y_\partial(\mathtt{S}, t)$.

4. Structure-preserving mixed FEM discretization

In this section, we propose a structure-preserving, nonlinear mixed finite element discretization based on three fields. The approach is derived from a virtual power principle rooted in the GHP, enabling the derivation of finite-dimensional nonlinear PHS models. It is assumed that the interpolation spaces for the generalized displacement, strain, and stress fields are appropriately selected to ensure consistency and accuracy of the discretized system. A brief discussion on the choice of these interpolation is provided later in the section.

Proposition 4 (Weak form). The weak form of the nonlinear PHS (33), following the virtual power principle derived from the GHP, is given by:

$$\delta P_p = \int_\Omega \delta\dot{r} \cdot [\,\dot{p} + \mathcal{F}_\mathtt{X}(r)^* e_\epsilon - b - B_d\, u_d]\, d\mathtt{X} + \int_{\partial\Omega_N} \delta\dot{r} \cdot [F_\partial(r)\, e_\epsilon - \tau_N]\, d\mathtt{S} = 0, \tag{39}$$

$$\delta P_e = \int_\Omega \delta e_\epsilon \cdot [\,\dot{\epsilon} - \mathcal{F}_\mathtt{X}(r)\, \dot{r}]\, d\mathtt{X} + \int_{\partial\Omega_D} \delta e_\epsilon \cdot F_\partial(r)^\top (\dot{r} - v_D)\, d\mathtt{S} = 0, \tag{40}$$

$$\delta P_\epsilon = \int_\Omega \delta\dot{\epsilon} \cdot \left(e_\epsilon - \frac{\partial \Psi}{\partial \epsilon} \right) d\mathtt{X} = 0, \tag{41}$$

where δP_p, δP_e, and δP_ϵ represent the virtual powers associated with the variations $\delta\dot{r}$, δe_ϵ, and $\delta\dot{\epsilon}$, respectively.

Proof. The details of the proof are provided in Appendix A. □

Theorem 2 (Structure-preserving mixed FEM). The structure-preserving mixed FEM discretization of (33) based on the weak formulation in Proposition 4, using the approximations:

$$\begin{aligned}
&\tilde{r}(\mathtt{X},t) = N_r(\mathtt{X})\,\hat{r}(t), && \delta\tilde{r}(\mathtt{X},t) = N_r(\mathtt{X})\,\delta\hat{r}(t), && \tilde{v}_D(\mathtt{S},t) = N_{v_D}(\mathtt{S})\,\hat{v}_D(t),\\
&\tilde{e}_\epsilon(\mathtt{X},t) = N_e(\mathtt{X})\,\hat{e}(t), && \delta\tilde{e}_\epsilon(\mathtt{X},t) = N_e(\mathtt{X})\,\delta\hat{e}(t), && \tilde{\tau}_N(\mathtt{S},t) = N_{\tau_N}(\mathtt{S})\,\hat{\tau}_N(t),\\
&\tilde{\epsilon}(\mathtt{X},t) = N_\epsilon(\mathtt{X})\,\hat{\epsilon}(t), && \delta\tilde{\epsilon}(\mathtt{X},t) = N_\epsilon(\mathtt{X})\,\delta\hat{\epsilon}(t), && \tilde{u}_d(\mathtt{X},t) = N_{u_d}(\mathtt{X})\,\hat{u}_d(t),
\end{aligned} \tag{42}$$

with $N_r(\mathtt{X})$, $N_e(\mathtt{X}) = N_\epsilon(\mathtt{X})$, $N_{u_d}(\mathtt{X})$, $N_{v_D}(\mathtt{S})$ and $N_{\tau_N}(\mathtt{S})$ properly selected interpolation shape functions, leads to the finite-dimensional nonlinear PHS of the form:

$$\underbrace{\begin{bmatrix}\dot{\hat{p}}(t)\\ \dot{\hat{\epsilon}}(t)\\ \dot{\hat{r}}(t)\end{bmatrix}}_{\dot{\hat{x}}(t)} = \underbrace{\begin{bmatrix}0 & -\hat{F}_x(\hat{r})^\top & -I\\ \hat{F}_x(\hat{r}) & 0 & 0\\ I & 0 & 0\end{bmatrix}}_{\hat{J}(\hat{x})=-\hat{J}(\hat{x})^\top} \underbrace{\begin{bmatrix}\hat{e}_p(t)\\ \hat{e}_\epsilon(\hat{\epsilon})\\ -\hat{b}\end{bmatrix}}_{\nabla_{\hat{x}}\hat{H}(\hat{x})} + \underbrace{\begin{bmatrix}\hat{B}_d & \hat{B}_N & 0\\ 0 & 0 & \hat{B}_D(\hat{r})\\ 0 & 0 & 0\end{bmatrix}}_{\hat{G}(\hat{x})} \underbrace{\begin{bmatrix}\hat{u}_d(t)\\ \hat{\tau}_N(t)\\ \hat{v}_D(t)\end{bmatrix}}_{\hat{u}(t)} \tag{43}$$

$$\hat{y}(t) = \hat{G}(\hat{x})^\top \nabla_{\hat{x}}\hat{H}(\hat{x}) = \begin{bmatrix}\hat{B}_d^\top\,\hat{e}_p(t)\\ \hat{B}_N^\top\,\hat{e}_p(t)\\ \hat{B}_D(\hat{r})^\top\,\hat{e}_\epsilon(\hat{\epsilon})\end{bmatrix} = \begin{bmatrix}\hat{y}_d(t)\\ \hat{v}_N(t)\\ \hat{\tau}_D(t)\end{bmatrix},$$

$$\hat{H}(\hat{x}) = \frac{1}{2}\,\hat{p}(t)^\top \hat{M}^{-1}\hat{p}(t) + \hat{U}(\hat{\epsilon}) - \hat{r}(t)^\top \hat{b}, \tag{44}$$

$$\dot{\hat{H}} = \hat{u}(t)^\top \hat{y}(t), \tag{45}$$

where $\hat{e}_p(t) = \hat{M}^{-1}\hat{p}(t)$ is the discrete generalized velocity, $\hat{e}_\epsilon(\hat{\epsilon}) = \nabla_{\hat{\epsilon}}\hat{U}(\hat{\epsilon})$ is the discrete generalized stress, and I is an identity matrix. The discrete elastic energy $\hat{U}(\hat{\epsilon})$ and the involved matrices and vectors are defined as:

$$\hat{U}(\hat{\epsilon}) = \int_\Omega \Psi(N_\epsilon(\mathtt{X})\,\hat{\epsilon}(t))\,d\mathtt{X}, \tag{46}$$

$$\hat{e}_\epsilon(\hat{\epsilon}) = \int_\Omega \left(N_\epsilon(\mathtt{X})^\top \frac{\partial \Psi}{\partial \epsilon}\Big|_{\epsilon=\tilde{\epsilon}} \right) d\mathtt{X}, \tag{47}$$

$$\hat{M}_e = \int_\Omega N_e(\mathtt{X})^\top N_\epsilon(\mathtt{X})\,d\mathtt{X}, \tag{48}$$

$$\hat{\Sigma}(\hat{r}) = \int_\Omega N_e(\mathtt{X})^\top (\mathcal{F}_{\mathtt{X}}(\tilde{r})N_r(\mathtt{X}))\,d\mathtt{X} - \int_{\partial\Omega_D} N_e(\mathtt{S})^\top F_\partial(\tilde{r})^\top N_r(\mathtt{S})\,d\mathtt{S}, \tag{49}$$

$$\hat{\Gamma}(\hat{r}) = \int_{\partial\Omega_D} N_e(\mathtt{S})^\top F_\partial(\tilde{r})^\top N_{v_D}(\mathtt{S})\,d\mathtt{S}, \tag{50}$$

$$\hat{B}_N = \int_{\partial\Omega_N} N_r(\mathtt{S})^\top N_{\tau_N}(\mathtt{S})\,d\mathtt{S}, \tag{51}$$

$$\hat{B}_d = \int_\Omega N_r(\mathtt{X})^\top B_d\,N_{u_d}(\mathtt{X})\,d\mathtt{X}, \tag{52}$$

$$\hat{M} = \int_\Omega N_r(\mathtt{X})^\top \mathcal{M}(\mathtt{X})\,N_r(\mathtt{X})\,d\mathtt{X}, \tag{53}$$

$$\hat{b} = \int_{\Omega} N_r(\mathtt{X})^\top \, b(\mathtt{X}) \, d\mathtt{X}, \tag{54}$$

where $\hat{F}_x(\hat{r}) = \hat{M}_e^{-1}\hat{\Sigma}(\hat{r})$ and $\hat{B}_D(\hat{r}) = \hat{M}_e^{-1}\hat{\Gamma}(\hat{r})$.

Proof. The proof follows by substituting the approximations into the weak formulation. Details are provided in Appendix A. □

Corollary 1. An alternative PHS representation of the finite-dimensional model in Theorem 2 is given by:

$$\underbrace{\begin{bmatrix} \hat{M} & 0 & 0 \\ 0 & \hat{M}_e & 0 \\ 0 & 0 & I \end{bmatrix}}_{\hat{E}} \underbrace{\begin{bmatrix} \dot{\hat{v}}(t) \\ \dot{\hat{\epsilon}}(t) \\ \dot{\hat{r}}(t) \end{bmatrix}}_{\dot{\hat{\xi}}(t)} = \underbrace{\begin{bmatrix} 0 & -\hat{\Sigma}(\hat{r})^\top & -I \\ \hat{\Sigma}(\hat{r}) & 0 & 0 \\ I & 0 & 0 \end{bmatrix}}_{\hat{J}_\xi(\hat{\xi}) = -\hat{J}_\xi(\hat{\xi})^\top} \underbrace{\begin{bmatrix} \hat{v}(t) \\ \hat{e}(\hat{\epsilon}) \\ -\hat{b} \end{bmatrix}}_{\hat{Z}(\hat{\xi})} + \underbrace{\begin{bmatrix} \hat{B}_d & \hat{B}_N & 0 \\ 0 & 0 & \hat{\Gamma}(\hat{r}) \\ 0 & 0 & 0 \end{bmatrix}}_{\hat{G}_\xi(\hat{\xi})} \underbrace{\begin{bmatrix} \hat{u}_d(t) \\ \hat{\tau}_N(t) \\ \hat{v}_D(t) \end{bmatrix}}_{\hat{u}(t)} \tag{55}$$

$$\hat{y}(t) = \hat{G}_\xi(\hat{\xi})^\top \hat{Z}(\hat{\xi}) = \begin{bmatrix} \hat{B}_d^\top \hat{v}(t) \\ \hat{B}_N^\top \hat{v}(t) \\ \hat{\Gamma}(\hat{r})^\top \hat{e}(\hat{\epsilon}) \end{bmatrix} = \begin{bmatrix} \hat{y}_d(t) \\ \hat{v}_N(t) \\ \hat{\tau}_D(t) \end{bmatrix},$$

$$\hat{H}(\hat{\xi}) = \frac{1}{2}\hat{v}(t)^\top \hat{M}\,\hat{v}(t) + \hat{U}(\hat{\epsilon}) - \hat{r}(t)^\top \hat{b}, \tag{56}$$

$$\dot{\hat{H}} = \hat{u}(t)^\top \hat{y}(t), \tag{57}$$

where $\nabla_{\hat{\xi}}\hat{H}(\hat{\xi}) = \hat{E}^\top \hat{Z}(\hat{\xi})$ is the gradient of the Hamiltonian, $\hat{v}(t) = \dot{\hat{r}}(t)$ is the discrete generalized velocity, and $\hat{e}(\hat{\epsilon}) = \hat{M}_e^{-\top}\hat{e}_\epsilon(\hat{\epsilon})$ is the discretized stress.

In the formulation of Corollary 1, the velocity $\hat{v}(t)$ is introduced as a state variable in place of the momentum $\hat{p}(t)$. This leads to an equivalent PHS while avoiding the need to compute $\hat{M}^{-1}$. In addition, in Theorem 2 and Corollary 1, preserving the PHS structure depends on the invertibility of the matrix $\hat{M}_e$ in (48), which couples the strain and stress interpolation spaces. Since invertibility may not hold for arbitrary shape function choices, we impose the condition that both fields share the same interpolation, i.e., $N_e(\mathtt{X}) = N_\epsilon(\mathtt{X})$. In this context, we emphasize that the selection of interpolation spaces may depend on the specific spatial dimension and the nature of the nonlinearity. For instance, the linear case, characterized by infinitesimal strains and Hookean material, can be seen as a particular case in which greater flexibility in the choice of interpolation spaces is possible. However, for nonlinear elasticity, standard practice suggests using continuous piecewise linear shape functions for displacements, and discontinuous piecewise constant shape functions for stresses and strains, in order to ensure both numerical stability and accuracy [57, 58].

An important feature of the proposed finite-dimensional port-Hamiltonian formulations is that generalized stresses, strains, and displacements are treated as independent fields. This approach eliminates the need to invert the hyperelastic (nonlinear) constitutive relation, which is advantageous for general hyperelastic materials where the stress-strain relationship may not be uniquely invertible [59]. Inversion-based methods are more commonly associated with Hellinger-Reissner-type formulations [60], for which a port-Hamiltonian variant has been developed in [30], albeit restricted to materially linear systems. While certain strategies allow the constitutive relation to be inverted by selecting appropriate solution branches [60], extending the present port-Hamiltonian framework to such cases lies beyond the scope of this work and represents an interesting direction for future research. It is also important to mention the issue of volumetric locking, a well-known numerical artifact that can arise when modeling nearly incompressible materials. Although this work does not explicitly address locking, the formulation's treatment of generalized strains as independent fields is, in principle, compatible with extensions that incorporate enhanced strain modes to alleviate such effects, as in [61, 62]. Integrating these techniques into the proposed approach remains an open and valuable avenue for further investigation.

One potential limitation of the proposed finite-dimensional models is their applicability to static problems. From a control-theoretic perspective, the equilibrium points (i.e., static solutions) of the system cannot be directly characterized within the current formulation. To illustrate this, let $\hat{x}^* = [\hat{p}^{*\top}\ \hat{\epsilon}^{*\top}\ \hat{r}^{*\top}]^\top$ and $\hat{u}^* = [\hat{u}_d^{*\top}\ \hat{\tau}_N^{*\top}\ \hat{v}_D^{*\top}]^\top$ denote the equilibrium state and input vectors, respectively, under the assumption $\dot{\hat{x}} = 0$. This leads to the following set of equations:

$$0 = -\hat{F}_x(\hat{r}^*)^\top \hat{e}_\epsilon(\hat{\epsilon}^*) + \hat{b} + \hat{B}_d \hat{u}_d^* + \hat{B}_N \hat{\tau}_N^* \tag{58}$$

$$0 = \hat{F}_x(\hat{r}^*)\hat{M}^{-1}\hat{p}^* + \hat{B}_D(\hat{r}^*)\hat{v}_D^* \tag{59}$$

$$0 = \hat{M}^{-1}\hat{p}^*. \tag{60}$$

As expected, (60) implies that $\hat{p}^* = 0$ (or $\hat{v}^* = 0$ in the model of Corollary 1). Substituting this into (59), and noticing that $\hat{v}_D^* = 0$ at equilibrium, results in an identity of the form $0 = 0$, rendering the equation uninformative. Consequently, only (58) remains to implicitly characterize equilibrium points in terms of $\hat{\epsilon}^*$ and $\hat{r}^*$. This issue arises because the kinematic relation is introduced in rate form, meaning that no algebraic equation directly links generalized strains and displacements. To overcome this, we propose to augment the finite-dimensional PHS models with an additional equation: a discretized version of the kinematic relation, derived from the virtual work principle underlying the GHP.

Proposition 5 (Kinematic equation). Consider the infinite-dimensional PHS of Theorem 1. The weak form of the kinematic equation is given by:

$$\int_\Omega \delta e_\epsilon \cdot [\epsilon - \epsilon(r)]\, d\mathtt{X} + \int_{\partial\Omega_D} \delta e_\epsilon \cdot F_\partial(r)^\top (r - r_D)\, d\mathtt{S} = 0, \tag{61}$$

which represents the virtual work associated with the variation δe_ϵ, where $\epsilon(r) \in \mathbb{R}^m$ denotes the continuous generalized strain expressed in terms of $r(\mathtt{X}, t)$. Using the approximations introduced in (42), along with $\tilde{r}_D(\mathtt{S}, t) = N_{v_D}(\mathtt{S})\,\hat{r}_D(t)$, this leads to the following discretized kinematic relation:

$$\hat{\epsilon}(t) = \hat{\epsilon}(\hat{r}) + \hat{B}_D(\hat{r})\hat{r}_D(t), \tag{62}$$

where $\hat{\epsilon}(\hat{r}) = \hat{M}_e^{-1}(\hat{\Phi}(\hat{r}) - \hat{\Upsilon}(\hat{r})\hat{r})$, with $\hat{\Phi}(\hat{r})$ and $\hat{\Upsilon}(\hat{r})$ defined by:

$$\hat{\Phi}(\hat{r}) = \int_\Omega N_e(\mathtt{X})^\top \epsilon(\tilde{r})\, d\mathtt{X}, \tag{63}$$

$$\hat{\Upsilon}(\hat{r}) = \int_{\partial\Omega_D} N_e(\mathtt{S})^\top F_\partial(\tilde{r})^\top N_r(\mathtt{S})\, d\mathtt{S}. \tag{64}$$

Proof. The details of the proof are provided in Appendix A. □

Evaluating the proposed equation (62) at equilibrium, i.e., $\hat{\epsilon}^* = \hat{\epsilon}(\hat{r}^*) + \hat{B}_D(\hat{r}^*)\hat{r}_D^*$, together with (58) and (60), yields a system of equations that can be solved to determine the equilibrium points, given the known stationary inputs $\hat{u}_d^*$, $\hat{\tau}_N^*$, and $\hat{r}_D^*$.

5. Examples

In this section, two examples illustrate the applicability and effectiveness of the proposed framework for multidimensional PHS modeling and mixed finite element discretization. The first example considers a one-dimensional beam modeled with Saint Venant–Kirchhoff material and von Kármán strain assumptions, aimed at validating the static formulation. The second example analyzes the dynamic response of a two-dimensional frame composed of compressible Neo–Hookean material and governed by full Green–Lagrange strains.

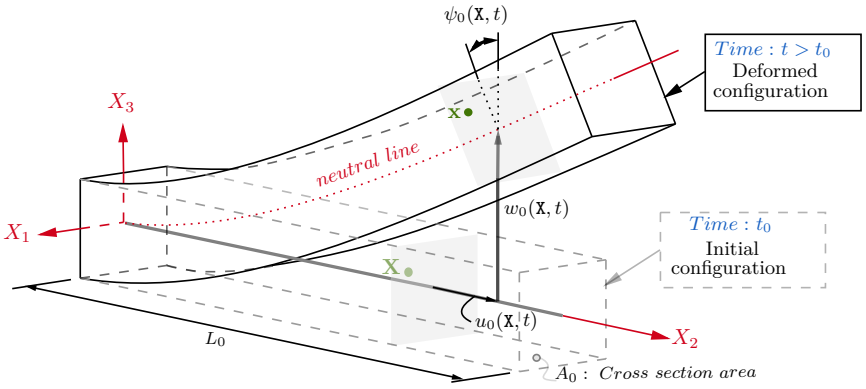

Figure 4: Beam configurations.

5.1. One-dimensional planar Timoshenko beam

The Timoshenko beam model is based on the kinematic assumption that plane sections perpendicular to the neutral line before deformation remain plane but are not necessarily perpendicular to the neutral line after deformation [63, Chapter 10.1]. Figure 4 shows the initial and deformed configurations. Let $\mathbf{X}$ be an arbitrary material point with coordinates $\mathbf{X} = [X_1\ X_2\ X_3]^\top$. Since plane sections remain plane, the position $\mathbf{X}$ in the deformed configuration has coordinates $\mathbf{x} = \mathbf{x}(\mathbf{X}, t)$ given by:

$$\mathbf{x}(\mathbf{X},t) = \begin{bmatrix} X_1 \\ X_2 + u_0(X_2,t) - X_3\sin(\psi_0(X_2,t)) \\ w_0(X_2,t) + X_3\cos(\psi_0(X_2,t)) \end{bmatrix} \approx \begin{bmatrix} X_1 \\ X_2 + u_0(X_2,t) - X_3\,\psi_0(X_2,t) \\ w_0(X_2,t) + X_3 \end{bmatrix},$$

where the usual approximations $\sin(\psi_0) \approx \psi_0$ and $\cos(\psi_0) \approx 1$ are used. Then, the kinematic assumption of the Timoshenko beam is equivalent to the displacement field $\mathbf{u}(\mathbf{X}, t) \in \mathbb{R}^3$ given by:

$$\mathbf{u}(\mathbf{X},t) = \mathbf{x}(\mathbf{X},t) - \mathbf{X} = \begin{bmatrix} 0 \\ u_0(X_2,t) - X_3\,\psi_0(X_2,t) \\ w_0(X_2,t) \end{bmatrix} = \underbrace{\begin{bmatrix} 0 & 0 & 0 \\ 1 & -X_3 & 0 \\ 0 & 0 & 1 \end{bmatrix}}_{\bar{M}_1(\mathtt{X}^c)} \underbrace{\begin{bmatrix} u_0(\mathtt{X},t) \\ \psi_0(\mathtt{X},t) \\ w_0(\mathtt{X},t) \end{bmatrix}}_{r(\mathtt{X},t)},$$

where $\mathtt{X} = \{X_2\}$, $\mathtt{X}^c = \{X_1, X_3\}$, $\Omega = (0, L_0) \subset \mathbb{R}$ with L_0 the initial length of the beam, $\Omega^c = A_0 \subset \mathbb{R}^2$ with $A_0(\mathtt{X})$ the initial cross section area, $u_0(\mathtt{X}, t)$ and $w_0(\mathtt{X}, t)$ are the axial and vertical displacements of points belonging to the neutral axis, respectively, and $\psi_0(\mathtt{X}, t)$ is the angle rotated by the cross section. Hyperelastic material behavior is modeled using the Saint Venant–Kirchhoff model, where the strain energy density function is given by:

$$W(\underline{\mathbf{E}}) = \frac{1}{2}\left(\underline{\underline{C_L}} : \underline{\mathbf{E}}\right) : \underline{\mathbf{E}},$$

with $\underline{\underline{C_L}} : \mathbb{R}^{3\times3} \to \mathbb{R}^{3\times3}$ the isotropic fourth-order constitutive tensor given by:

$$\underline{\underline{C_L}} = 2\mu_L \underline{\underline{\mathcal{I}_S}} + \lambda_L \underline{I} \otimes \underline{I},$$

where $\underline{\underline{\mathcal{I}_S}}$ is the symmetric fourth-order identity tensor, and μ_L, $\lambda_L \in \mathbb{R}$ are the Lamé constants of the material given by:

$$\mu_L = \frac{E}{2(1+\nu)} = G, \quad \lambda_L = \frac{\nu E}{(1+\nu)(1-2\nu)},$$

where E is Young's modulus, ν is Poisson's ratio, and $\mu_L = G$ is also known as the shear modulus.

5.1.1. Port-Hamiltonian modeling

To obtain the infinite-dimensional PHS model we apply the Procedure stated in Section 3.3.

Step 1. From Proposition 1, and assuming that the cross section is symmetric with respect to its centroidal coordinates, the mass density matrix $\mathcal{M}(\mathtt{X}) \in \mathbb{R}^{3\times 3}$ is given by:

$$\mathcal{M}(\mathtt{X}) = \rho_0(\mathtt{X}) \int_{\Omega^c} \bar{M}_1(\mathtt{X}^c)^\top \bar{M}_1(\mathtt{X}^c)\, d\mathtt{X}^c = \begin{bmatrix} \rho_0(\mathtt{X})A_0(\mathtt{X}) & 0 & 0 \\ 0 & \rho_0(\mathtt{X})I_2(\mathtt{X}) & 0 \\ 0 & 0 & \rho_0(\mathtt{X})A_0(\mathtt{X}) \end{bmatrix},$$

with $I_2(\mathtt{X}) \in \mathbb{R}$ the second moment of inertia of the cross section. Then, the generalized momentum $p(\mathtt{X}, t) \in \mathbb{R}^3$, the kinetic energy $T(p) \in \mathbb{R}$ and the co-energy variable $e_p(\mathtt{X}, t) \in \mathbb{R}^3$ are completely defined.

Step 2. The components of the Green–Lagrange strain tensor are obtained from (8). Then, the nonzero components of the Voigt-strain vector are given by:

$$\begin{aligned} E_{22} &= (\partial_2 u_0 - X_3 \partial_2 \psi_0) + \frac{1}{2}(\partial_2 u_0 - X_3 \partial_2 \psi_0)^2 + \frac{1}{2}(\partial_2 w_0)^2, \\ 2E_{23} &= (\partial_2 w_0 - \psi_0) - \psi_0(\partial_2 u_0 - X_3 \partial_2 \psi_0), \\ E_{33} &= \frac{1}{2}\psi_0^2. \end{aligned}$$

Applying the von Kármán strain approximation, that is, neglecting nonlinear stretching terms, these expressions simplify to:

$$\underbrace{\begin{bmatrix} E_{22} \\ 2E_{23} \end{bmatrix}}_{\boldsymbol{\varepsilon}(\mathbf{X},t)} = \underbrace{\begin{bmatrix} 1 & -X_3 & 0 \\ 0 & 0 & 1 \end{bmatrix}}_{\bar{M}_2(\mathtt{X}^c)} \underbrace{\begin{bmatrix} \partial_2 u_0 + \frac{1}{2}(\partial_2 w_0)^2 \\ \partial_2 \psi_0 \\ \partial_2 w_0 - \psi_0 \end{bmatrix}}_{\epsilon(\mathtt{X},t)}.$$

With the above, the generalized strains $\epsilon(\mathtt{X}, t) \in \mathbb{R}^3$, as well as its time derivative $\dot{\epsilon}(\mathtt{X}, t)$, are expressed as:

$$\begin{bmatrix} \epsilon_1 \\ \epsilon_2 \\ \epsilon_3 \end{bmatrix} = \underbrace{\begin{bmatrix} \partial_2 u_0 + \frac{1}{2}(\partial_2 w_0)^2 \\ \partial_2 \psi_0 \\ \partial_2 w_0 - \psi_0 \end{bmatrix}}_{\epsilon(r)} \quad \rightarrow \quad \begin{bmatrix} \dot{\epsilon}_1 \\ \dot{\epsilon}_2 \\ \dot{\epsilon}_3 \end{bmatrix} = \underbrace{\begin{bmatrix} \partial_2 & 0 & \partial_2 w_0 \partial_2 \\ 0 & \partial_2 & 0 \\ 0 & -1 & \partial_2 \end{bmatrix}}_{\mathcal{F}_\mathtt{X}(r)} \begin{bmatrix} \dot{u}_0 \\ \dot{\psi}_0 \\ \dot{w}_0 \end{bmatrix},$$

where the associated matrices of the differential operator $\mathcal{F}_\mathtt{X}(r)$ are given by:

$$F_0 = \begin{bmatrix} 0 & 0 & 0 \\ 0 & 0 & 0 \\ 0 & -1 & 0 \end{bmatrix}, \qquad F_2(r) = \begin{bmatrix} 1 & 0 & \partial_2 w_0 \\ 0 & 1 & 0 \\ 0 & 0 & 1 \end{bmatrix}.$$

Finally, the formal adjoint operator $\mathcal{F}_\mathtt{X}(r)^*$ is obtained in accordance with Definition 3.

Step 3. Considering that only remain $\boldsymbol{\varepsilon}(\mathbf{X}, t) \in \mathbb{R}^2$, the strain energy density function of the Saint Venant–Kirchhoff material can be rewritten as:

$$W(\boldsymbol{\varepsilon}) = \frac{1}{2}\boldsymbol{\varepsilon}^\top C_L\, \boldsymbol{\varepsilon} = \frac{1}{2}\begin{bmatrix} E_{22} \\ 2E_{23} \end{bmatrix}^\top \underbrace{\begin{bmatrix} E & 0 \\ 0 & \kappa G \end{bmatrix}}_{C_L} \begin{bmatrix} E_{22} \\ 2E_{23} \end{bmatrix},$$

where κ is a correction factor and C_L is the constitutive matrix. Since $\boldsymbol{\varepsilon}(\mathbf{X},t) = \bar{M}_2(\mathtt{X}^c)\epsilon(\mathtt{X},t)$, the generalized strain energy density function $\Psi(\epsilon)$ is obtained from (24) and is given by:

$$\Psi(\epsilon) = \frac{1}{2}\,\epsilon(\mathtt{X},t)^\top \underbrace{\int_{\Omega^c} \bar{M}_2(\mathtt{X}^c)^\top C_L \bar{M}_2(\mathtt{X}^c)\, d\mathtt{X}^c}_{\mathcal{K}_\epsilon(\mathtt{X})}\, \epsilon(\mathtt{X},t) = \frac{1}{2} \underbrace{\begin{bmatrix}\epsilon_1\\ \epsilon_2\\ \epsilon_3\end{bmatrix}^\top}_{\epsilon(\mathtt{X},t)} \underbrace{\begin{bmatrix} EA_0(\mathtt{X}) & 0 & 0\\ 0 & EI_2(\mathtt{X}) & 0\\ 0 & 0 & \kappa G A_0(\mathtt{X})\end{bmatrix}}_{\mathcal{K}_\epsilon(\mathtt{X})} \underbrace{\begin{bmatrix}\epsilon_1\\ \epsilon_2\\ \epsilon_3\end{bmatrix}}_{\epsilon(\mathtt{X},t)},$$

where $\mathcal{K}_\epsilon(\mathtt{X})$ is the stiffness density matrix. Then, the elastic energy $U(\epsilon)$ and the co-energy variables $e_\epsilon(\mathtt{X},t)$ are completely defined.

Step 4. The generalized distributed load and body force are not included in this example.

Step 5. From Theorem 1, the infinite-dimensional nonlinear PHS, the Hamiltonian, and boundary inputs and outputs are completely defined.

Note that the PHS model derived here coincides with the formulation proposed in [27], illustrating the ability of the proposed methodology to systematically recover known models. Moreover, by selecting different combinations of strain measures (e.g., infinitesimal, von Kármán, or GreenLagrange) and constitutive hyperelastic laws, new models can be readily derived.

5.1.2. FEM discretization and static solutions

The previously derived model is now employed to test the proposed mixed finite element method in a static setting. The beam under consideration is characterized by the following physical parameters: $L_0 = 0.5$ [m], $A_0 = 3\times10^{-5}$ [m^2], $I_2 = 2.5\times10^{-12}$ [m^4], $\rho_0 = 7800$ [kg/m^3], $E = 210$ [GPa], $\nu = 0.3$ [-], and $\kappa = 5/6$ [-]. Homogeneous Dirichlet boundary conditions are imposed at $\mathtt{S} = 0$, that is, $v_D(0,t) = 0$, while a non-homogeneous Neumann condition is applied at the opposite end:

$$\tau_N(L_0,t) = \begin{bmatrix}0\\ M_\circ(t)\\ 0\end{bmatrix},$$

where $M_\circ(t)$ denotes a bending moment. It is well known in the literature that when $M_\circ = \alpha 2\pi EI_2/L_0$, with $\alpha \in [0,1]$, the beam is expected, according to the exact deformation theory, to deform into an arc of a circle of radius $R_\circ = EI_2/M_\circ$. Here, the parameter α characterizes the deformation stage, with $\alpha = 0$ corresponding to the undeformed (straight) beam, and $\alpha = 1$ corresponding to the fully deformed circular beam. This benchmark allows us to assess the accuracy of the proposed mixed FEM formulation.

To evaluate the performance of the discretization, four test cases are considered. The first two cases use uniform meshes of five and ten elements, employing continuous first-order Lagrangian shape functions for the generalized displacements and discontinuous piecewise constant shape functions for the generalized stresses and strains; this combination is denoted as P1–P0. The other two test cases also use uniform meshes of five and ten elements, but employ continuous first-order Lagrangian shape functions for all field variables, denoted as P1–P1. Simulations are conducted for $\alpha = \{0,\ 0.05,\ 0.10,\ 0.15,\ 0.20,\ 0.25\}$. The set of equations (58) and (62) are solved in MATLAB using the `fsolve` function with the Levenberg-Marquardt algorithm. Each case converges in fewer than five iterations, with the full set of simulations completed in approximately 80 seconds. The results are shown in Fig. 5.

It should be recalled that the beam model is derived under the approximations $\sin(\psi_0) \approx \psi_0$ and $\cos(\psi_0) \approx 1$, along with von Kármán strains, which are valid under small strains and moderate rotations. Accordingly, the model is expected to reproduce the correct behavior in this regime. As shown in Fig. 5,

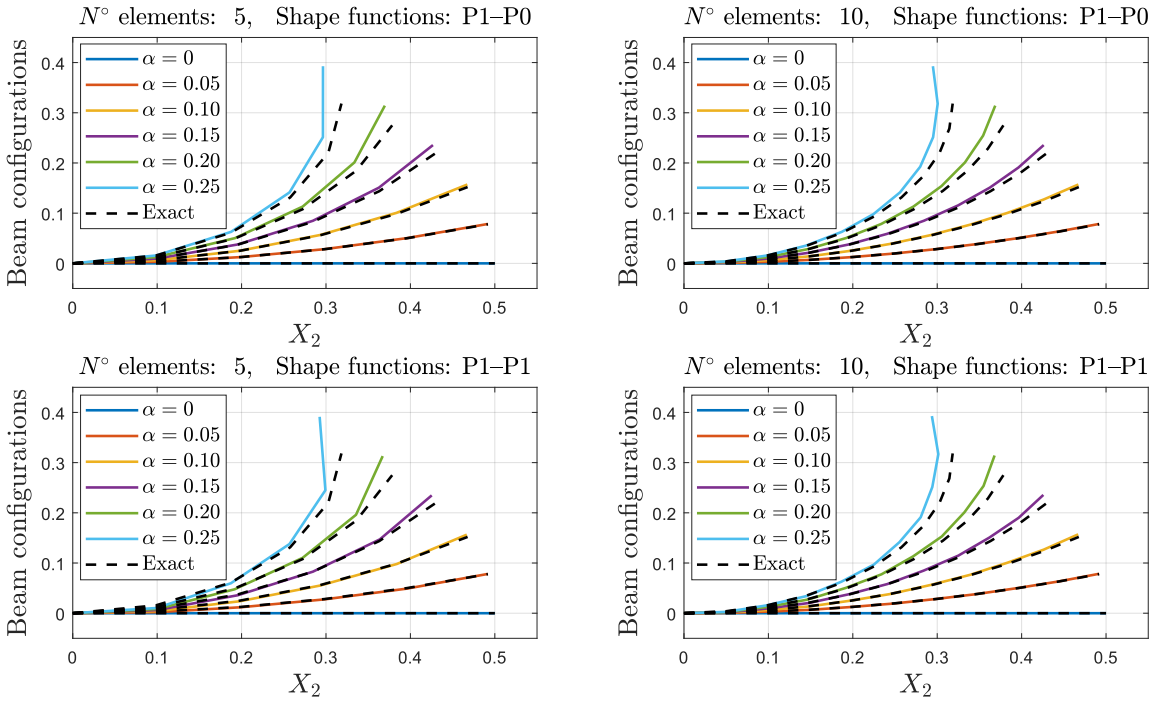

Figure 5: Static solutions of the beam for the four test cases.

axial and vertical displacements are coupled, consistent with the geometric nonlinearity of the model. The FEM-based results for the static problem exhibit excellent agreement with the exact solution for small values of α, confirming the model's validity within its intended range of application. In addition, all four test cases yield consistent results, with convergence toward the same static configuration as the mesh is refined, despite the different combinations of interpolation functions.

5.2. Two-dimensional elastic frame

To evaluate the dynamic capabilities of the proposed framework, we now consider a two-dimensional elasticity problem as a representative example. Consider the frame in Fig. 6, where $h \in \mathbb{R}$ represents the constant thickness. The displacement field for the two-dimensional elasticity problem is given by:

$$\mathbf{u}(\mathbf{X},t) = \underbrace{\begin{bmatrix} 1 & 0 \\ 0 & 1 \\ 0 & 0 \end{bmatrix}}_{\bar{M}_1} \underbrace{\begin{bmatrix} u_1(\mathtt{X},t) \\ u_2(\mathtt{X},t) \end{bmatrix}}_{r(\mathtt{X},t)}, \tag{65}$$

where $\mathtt{X} = \{X_1, X_2\}$, $\mathtt{X}^c = \{X_3\}$, $\Omega \subset \mathbb{R}^2$, $\Omega^c = \left(-\frac{h}{2}, \frac{h}{2}\right) \subset \mathbb{R}$, and $u_1(\mathtt{X},t) \in \mathbb{R}$ and $u_2(\mathtt{X},t) \in \mathbb{R}$ are the displacements in the direction of the axes X_1 and X_2, respectively. Hyperelastic material behavior is modeled using the compressible Neo–Hookean model, where the strain energy density function is given by:

$$W(\underline{\mathbf{C}}) = \frac{\mu_L}{2}\left[I_C - 3 - \ln\left(III_C\right)\right] + \frac{\lambda_L}{2}\left(\sqrt{III_C} - 1\right)^2,$$

where μ_L, $\lambda_L \in \mathbb{R}$ are the Lamé constants of the material, and $I_C = \mathrm{tr}(\underline{\mathbf{C}}) \in \mathbb{R}$ and $III_C = \det(\underline{\mathbf{C}}) \in \mathbb{R}$ are the first and third invariants of the right Cauchy–Green deformation tensor $\underline{\mathbf{C}} = 2\underline{\mathbf{E}} + \underline{\mathbf{I}}$.

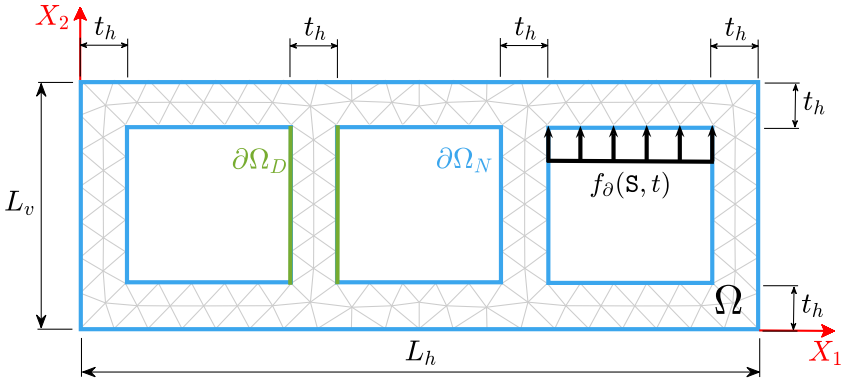

Figure 6: Two dimensional frame

5.2.1. Port-Hamiltonian modeling

To obtain the infinite-dimensional PHS model we apply the Procedure stated in Section 3.3.

Step 1. From Proposition 1:

$$\mathcal{M}(\mathtt{X}) = \rho_0(\mathtt{X}) \int_{\Omega^c} \bar{M}_1^\top \bar{M}_1 \, d\mathtt{X}^c = \begin{bmatrix} \rho_0(\mathtt{X})h & 0 \\ 0 & \rho_0(\mathtt{X})h \end{bmatrix}.$$

Then, the generalized momentum $p(\mathtt{X},t) \in \mathbb{R}^2$, the kinetic energy $T(p) \in \mathbb{R}$ and the co-energy variable $e_p(\mathtt{X},t) \in \mathbb{R}^2$ are completely defined.

Step 2. The components of the Green–Lagrange strain tensor are obtained from (8). Then, the nonzero components $\boldsymbol{\varepsilon}(\mathbf{X},t) \in \mathbb{R}^3$ of the Voigt-strain vector are:

$$\begin{aligned} E_{11} &= \partial_1 u_1 + \frac{1}{2}(\partial_1 u_1)^2 + \frac{1}{2}(\partial_1 u_2)^2 = \epsilon_1, \\ E_{22} &= \partial_2 u_2 + \frac{1}{2}(\partial_2 u_1)^2 + \frac{1}{2}(\partial_2 u_2)^2 = \epsilon_2, \\ 2E_{12} &= \partial_2 u_1 + \partial_1 u_2 + (\partial_1 u_1\, \partial_2 u_1) + (\partial_1 u_2\, \partial_2 u_2) = \epsilon_3, \end{aligned}$$

where the generalized strains are defined as $\epsilon = [E_{11}\ E_{22}\ 2E_{12}]^\top$. Taking the time derivative of $\epsilon(\mathtt{X},t) \in \mathbb{R}^3$ we obtain:

$$\begin{bmatrix} \dot{\epsilon}_1 \\ \dot{\epsilon}_2 \\ \dot{\epsilon}_3 \end{bmatrix} = \underbrace{\begin{bmatrix} \partial_1 + \partial_1 u_1 \partial_1 & \partial_1 u_2 \partial_1 \\ \partial_2 u_1 \partial_2 & \partial_2 + \partial_2 u_2 \partial_2 \\ \partial_2 + \partial_2 u_1 \partial_1 + \partial_1 u_1 \partial_2 & \partial_1 + \partial_2 u_2 \partial_1 + \partial_1 u_2 \partial_2 \end{bmatrix}}_{\mathcal{F}_\mathtt{X}(r)} \begin{bmatrix} \dot{u}_1 \\ \dot{u}_2 \end{bmatrix},$$

where the associated matrices of the differential operator $\mathcal{F}_\mathtt{X}(r)$ are given by:

$$F_1(r) = \begin{bmatrix} 1+\partial_1 u_1 & \partial_1 u_2 \\ 0 & 0 \\ \partial_2 u_1 & 1+\partial_2 u_2 \end{bmatrix}, \quad F_2(r) = \begin{bmatrix} 0 & 0 \\ \partial_2 u_1 & 1+\partial_2 u_2 \\ 1+\partial_1 u_1 & \partial_1 u_2 \end{bmatrix}.$$

Finally, the formal adjoint operator $\mathcal{F}_\mathtt{X}(r)^*$ is obtained in accordance with Definition 3.

Step 3. Considering the nonzero components of the Green–Lagrange strain tensor $\underline{\mathbf{E}}$, the right Cauchy–Green deformation tensor $\underline{\mathbf{C}}$ is given by:

$$\underline{\mathbf{C}}(\epsilon) = \begin{bmatrix} 2\epsilon_1 + 1 & \epsilon_3 & 0 \\ \epsilon_3 & 2\epsilon_2 + 1 & 0 \\ 0 & 0 & 1 \end{bmatrix},$$

so the invariants expressed in terms of the generalized strains are:

$$\begin{aligned} I_C(\epsilon) &= \operatorname{tr}(\underline{\mathbf{C}}(\epsilon)) = 2\epsilon_1 + 2\epsilon_2 + 3, \\ III_C(\epsilon) &= \det(\underline{\mathbf{C}}(\epsilon)) = (2\epsilon_1 + 1)(2\epsilon_2 + 1) - \epsilon_3^2. \end{aligned}$$

With the above, the generalized strain energy density function is given by $\Psi(\epsilon) = hW(\underline{\mathbf{C}}(\epsilon))$. Now, the co-energy variable $e_\epsilon(\mathtt{X}, t) \in \mathbb{R}^3$ is obtained by differentiation and we have:

$$e_\epsilon(\mathtt{X}, t) = \frac{\partial \Psi}{\partial \epsilon} = \frac{h\mu_L}{2}\frac{\partial I_C}{\partial \epsilon} - \frac{\partial III_C}{\partial \epsilon}\left(\frac{h\mu_L}{2III_C} - \frac{h\lambda_L}{2} + \frac{h\lambda_L}{2\sqrt{III_C}}\right).$$

Step 4. The generalized distributed load and body force are not included in this example.

Step 5. From Theorem 1, the infinite-dimensional nonlinear PHS, the Hamiltonian, and boundary inputs and outputs are completely defined.

Remark 6. If a different hyperelastic model is considered, the only requirement is to apply Step 3 for the new strain energy density function $W(\underline{\mathbf{E}})$. Consequently, if the kinematics remain unchanged, i.e., $\mathbf{u}(\mathbf{X}, t)$ and the strain measure do not change, Theorem 1 ensures that the new PHS model will have the same interconnection structure $\mathcal{J}(x) = -\mathcal{J}(x)^*$.

5.2.2. FEM discretization and time integration

The proposed mixed FEM discretization is now validated through numerical simulation. The following parameters are considered: $L_h = 30$ [cm], $L_v = 11$ [cm], $t_h = 2$ [cm], $h = 1$ [cm], $\rho_0 = 1000$ [kg/cm^3], $\mu_L = 17.8$ [kPa], and $\lambda_L = 71.5$ [kPa]. The discretization mesh follows the triangulation shown in Fig. 6, where continuous first-order Lagrangian shape functions are used for the generalized displacements, and discontinuous piecewise constant shape functions for the generalized stresses and strains. Homogeneous Dirichlet boundary conditions are applied, i.e., $v_D(\mathtt{S}, t) = 0$ for all $\mathtt{S} \in \partial\Omega_D$, along with non-homogeneous Neumann boundary conditions given by:

$$\tau_N(\mathtt{S}, t) = \begin{bmatrix} 0 \\ f_\partial(\mathtt{S}, t) \end{bmatrix} = \begin{bmatrix} 0 \\ 8.2\sin(50t) \end{bmatrix}, \text{ for } t < 0.5 \text{ [s]},$$

where $f_\partial(\mathtt{S}, t)$ [N/cm] represents a distributed boundary force applied only in the region indicated in Fig. 6.

To simulate the model, we consider two time integration schemes: an extended version of the Störmer–Verlet method [64], which provides an explicit scheme for the discretized PHS model, and the implicit midpoint rule, known for its enhanced stability and better energy behavior. In our implementation, the implicit midpoint method is initialized using the solution obtained from the extended Störmer–Verlet scheme, improving convergence speed. Details of this implementation are provided in Appendix B.

Remark 7. The Störmer–Verlet method and the implicit midpoint rule have been successfully combined in the context of geometrically nonlinear elastodynamics to achieve exact energy conservation and accelerated simulations [65, 66]. Although these approaches do not directly apply here due to material nonlinearity, recent developments in discrete gradient methods for port-Hamiltonian differential-algebraic equations [67] suggest promising directions for structure-preserving time integration of a broader class of nonlinear PHS, including those addressing hyperelasticity.

The simulation results are presented in Figs. 7 and 8, using a fixed time step $\Delta t = 2 \times 10^{-4}$ [s] and the initial condition $\hat{x}(0) = 0$. Fig. 7 shows the system configuration at different time instants. As expected, the frame remains fixed at the nodes where homogeneous Dirichlet BC are applied on $\partial\Omega_D$. Given that the initial condition is zero and neither distributed inputs nor self-weight are considered ($u_d(\mathtt{X}, t) = 0$ and $b(\mathtt{X}) = 0$, respectively), the system's dynamics is solely driven by the applied boundary traction, which ceases at $t = 0.5$ [s]. Since the system is conservative, the total energy should remain constant for $t \geq 0.5$ [s]. Both time integration methods yield similar results, with differences more clearly observed in the evolution of the total energy function $\hat{H}(\hat{x})$.

Fig. 8 shows that, while the Störmer–Verlet method performs adequately, it does not accurately capture the system's energy behavior after the input ceases. In contrast, the implicit midpoint rule more effectively preserves the system's energetic behavior, albeit at the cost of increased computational effort. To provide a quantitative comparison, the total simulation times were approximately 3.5 [hours] for the Störmer–Verlet method, 10 [hours] for the implicit midpoint rule initialized at each time step with the Störmer–Verlet solution, and 24 [hours] for the implicit midpoint method alone. These runtimes were obtained using a suboptimal MATLAB implementation, without parallelization or code-level optimization, aimed solely at validating the effectiveness of the proposed FEM approach. We are confident that significant reductions in computation time can be achieved through improved implementation strategies.

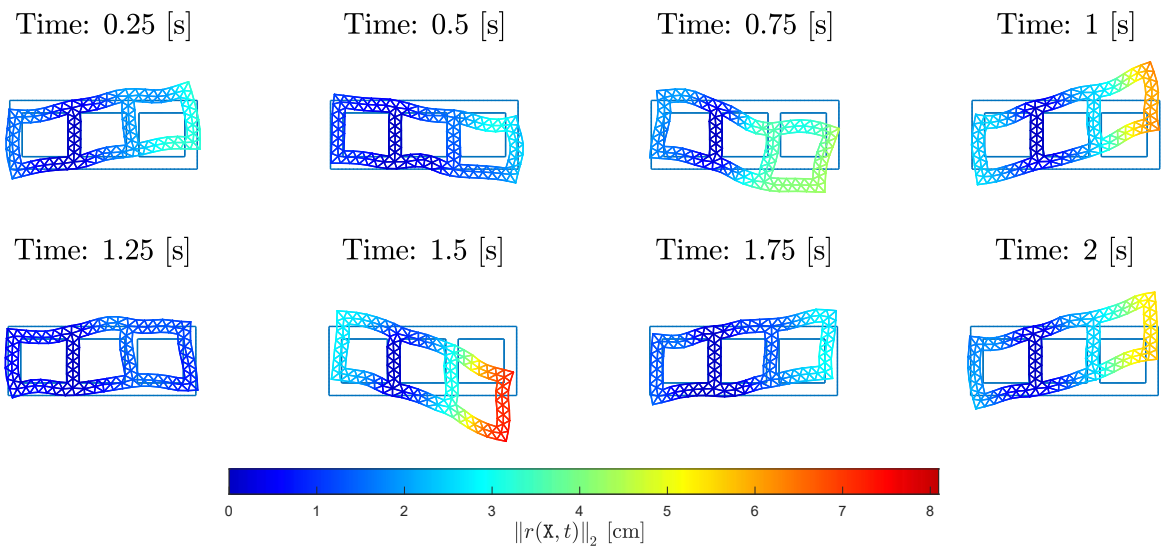

Figure 7: Time evolution of the configuration.

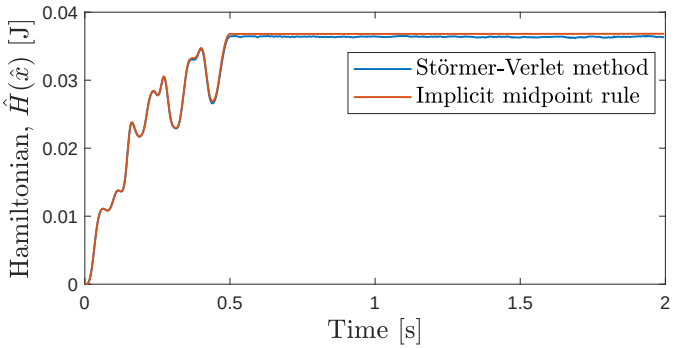

Figure 8: Hamiltonian function $\hat{H}(\hat{x})$.

6. Conclusion and perspectives

This paper presents a framework for modeling and FEM discretization of hyperelastic systems within the port-Hamiltonian formalism. The first contribution establishes a systematic methodology for modeling multidimensional nonlinear mechanical systems using the Generalized Hamilton's Principle. This approach provides a systematic and flexible framework capable of deriving infinite-dimensional PHS representations, enabling the rigorous treatment of large deformations and hyperelastic materials. The second contribution focuses on structure-preserving discretization using a mixed FEM approach with a three-field formulation. This method is proposed to preserve the intrinsic PHS structure of the system, ensuring physically consistent finite-dimensional approximations. Numerical simulations demonstrate the effectiveness of the proposed approach in accurately capturing the dynamic behavior of the underlying continuous system.

Future research may extend the proposed modeling framework to incorporate more complex physical phenomena, such as viscoelasticity [68] and electroelasticity [27, 69], thereby broadening its applicability to a wider range of engineering systems. The treatment of constrained systems, such as inextensible or incompressible formulations, is also of interest. In the context of discretization, nonlinear systems pose significant challenges due to the need for spatial integration and reassembly of system matrices at each time step. This complicates their use in control design, emphasizing the need for efficient simulation strategies. Potential advancements include the development of methods to accelerate computations and derive explicit global matrices, as explored in [65, 66] and [70, 71], respectively. These improvements could enhance the efficiency of simulations and facilitate the integration of the discretized models into control applications.

Acknowledgement

The authors acknowledge financial support from: Chilean ANID projects ECOS 220040, FONDECYT 1231896, BASAL AFB240002; the French projects EIPHI Graduate School ANR-17-EURE-0002, the IMPACTS Project ANR-21-CE48-0018; and the European MSCA Project MODCONFLEX 101073558.

Appendix A. Proofs

Proof of Theorem 1. The proof consists of applying the GHP. To improve the readability of the proof, it is divided into four steps and the spatial and temporal dependencies are omitted.

Step 1: From Proposition 1 we have $\mathcal{T} = \frac{1}{2}\int_\Omega \dot{r}^\top \mathcal{M}\dot{r}\, d\mathtt{X}$, then the term $\delta\int_{t_1}^{t_2} \mathcal{T}\, dt$ is given by:

$$\delta\int_{t_1}^{t_2} \mathcal{T}\, dt = \int_{t_1}^{t_2}\int_\Omega \delta\dot{r}^\top \mathcal{M}\dot{r}\, d\mathtt{X}\, dt,$$

where integrating by parts w.r.t. time we obtain:

$$\delta\int_{t_1}^{t_2} \mathcal{T}\, dt = \underbrace{\int_\Omega \delta r^\top \mathcal{M}\dot{r}\, d\mathtt{X}\Big|_{t_1}^{t_2}}_{=0 \text{ due to } (11)} - \int_{t_1}^{t_2}\int_\Omega \delta r^\top \mathcal{M}\ddot{r}\, d\mathtt{X}\, dt.$$

Step 2: Defining $\boldsymbol{\sigma}(\mathbf{X}, t) \in \mathbb{R}^d$ as the corresponding nonzero components of the Voigt-stress vector $\vec{T} = [T_{11}\ T_{22}\ T_{33}\ T_{12}\ T_{13}\ T_{23}]^\top \in \mathbb{R}^6$, where T_{ij} are the independent components of the second Piola–Kirchhoff stress tensor $\underline{\mathbf{T}}$, the extended elastic energy $\mathcal{U}_E$ defined in (13) is equivalent to:

$$\mathcal{U}_E = \int_{\mathcal{B}_0} [\boldsymbol{\sigma}\cdot(\boldsymbol{\varepsilon}(\mathbf{u}) - \boldsymbol{\varepsilon}) + W(\boldsymbol{\varepsilon})]\, d\mathbf{X}.$$

Noticing that $\delta\boldsymbol{\varepsilon}(\mathbf{u}) = \bar{M}_2\mathcal{F}_{\mathtt{X}}(r)\delta r$, then we have:

$$\delta\int_{t_1}^{t_2}\mathcal{U}_E\,dt = \int_{t_1}^{t_2}\int_{\mathcal{B}_0}\Big[\underbrace{\boldsymbol{\sigma}\cdot\delta\boldsymbol{\varepsilon}(\mathbf{u})}_{\boldsymbol{\sigma}^\top\bar{M}_2\mathcal{F}_{\mathtt{X}}\delta r} + \delta\boldsymbol{\sigma}\cdot(\boldsymbol{\varepsilon}(\mathbf{u})-\boldsymbol{\varepsilon}) - \delta\boldsymbol{\varepsilon}\cdot\left(\boldsymbol{\sigma}-\frac{\partial W(\boldsymbol{\varepsilon})}{\partial\boldsymbol{\varepsilon}}\right)\Big]\,d\mathbf{X}\,dt$$

$$= \int_{t_1}^{t_2}\Big[\int_\Omega\underbrace{\int_{\Omega^c}\boldsymbol{\sigma}^\top\bar{M}_2 d\mathtt{X}^c}_{e_\epsilon^\top}\mathcal{F}_{\mathtt{X}}\delta r\,d\mathtt{X} + \int_\Omega\underbrace{\int_{\Omega^c}\delta\boldsymbol{\sigma}^\top\bar{M}_2 d\mathtt{X}^c}_{\delta e_\epsilon^\top}(\epsilon(r)-\epsilon)\,d\mathtt{X}...$$

$$...-\int_\Omega\delta\epsilon^\top\Big(\underbrace{\int_{\Omega^c}\bar{M}_2^\top\boldsymbol{\sigma}\,d\mathtt{X}^c}_{e_\epsilon} - \underbrace{\int_{\Omega^c}\bar{M}_2^\top\frac{\partial W(\boldsymbol{\varepsilon})}{\partial\boldsymbol{\varepsilon}}d\mathtt{X}^c}_{\frac{\partial\Psi(\epsilon)}{\partial\epsilon}\text{ by Assumption 2}}\Big)\,d\mathtt{X}\Big]\,dt$$

$$= \int_{t_1}^{t_2}\Big[\underbrace{\int_\Omega e_\epsilon^\top\mathcal{F}_{\mathtt{X}}\delta r\,d\mathtt{X}}_{\text{Lemma 1}} + \int_\Omega\delta e_\epsilon^\top(\epsilon(r)-\epsilon)d\mathtt{X} - \int_\Omega\delta\epsilon^\top\left(e_\epsilon-\frac{\partial\Psi(\epsilon)}{\partial\epsilon}\right)d\mathtt{X}\Big]dt.$$

Applying Lemma 1 to the first term indicated above we obtain:

$$\int_\Omega e_\epsilon^\top\mathcal{F}_{\mathtt{X}}\delta r\,d\mathtt{X} = \int_\Omega\delta r^\top\mathcal{F}_{\mathtt{X}}^* e_\epsilon d\mathtt{X} + \int_{\partial\Omega_N}\delta r^\top F_\partial\,e_\epsilon\,d\mathtt{S} + \underbrace{\int_{\partial\Omega_D}\delta r^\top F_\partial\,e_\epsilon\,d\mathtt{S}}_{=0\text{ due to (10)}}.$$

Replacing the last expression into $\delta\int_{t_1}^{t_2}\mathcal{U}_E\,dt$ we obtain:

$$\delta\int_{t_1}^{t_2}\mathcal{U}_E\,dt = \int_{t_1}^{t_2}\Big\{\int_\Omega\Big[\delta r^\top\mathcal{F}_{\mathtt{X}}^* e_\epsilon + \delta e_\epsilon^\top(\epsilon(r)-\epsilon) - \delta\epsilon^\top\left(e_\epsilon-\frac{\partial\Psi(\epsilon)}{\partial\epsilon}\right)\Big]\,d\mathtt{X} + \int_{\partial\Omega_N}\delta r^\top F_\partial\,e_\epsilon\,d\mathtt{S}\Big\}dt.$$

Step 3: From Proposition (3) we derive:

$$\delta\int_{t_1}^{t_2}\mathcal{W}_E\,dt = \int_{t_1}^{t_2}\Big[\int_\Omega\delta r^\top(B_d\,u_d+b)d\mathtt{X} + \int_{\partial\Omega_N}\delta r^\top\tau_N\,d\mathtt{S} + \int_{\partial\Omega_D}\delta\tau_D^\top(r-r_D)d\mathtt{S}\Big]\,dt.$$

Step 4: Considering the above expressions, the application of the GHP leads to:

$$\int_{t_1}^{t_2}\delta(\mathcal{T}-\mathcal{U}_E+\mathcal{W}_E)dt = \int_{t_1}^{t_2}\Big\{\int_\Omega\Big[\delta r^\top\underbrace{(-\mathcal{M}\ddot{r}-\mathcal{F}_{\mathtt{X}}(r)^* e_\epsilon+b+B_d\,u_d)}_{(1)} - \delta e_\epsilon^\top\underbrace{(\epsilon(r)-\epsilon)}_{(2)} + \delta\epsilon^\top\underbrace{\left(e_\epsilon-\frac{\partial\Psi(\epsilon)}{\partial\epsilon}\right)}_{(3)}\Big]d\mathtt{X}\Big\}dt$$

$$...+\int_{t_1}^{t_2}\Big[\int_{\partial\Omega_N}\delta r^\top\underbrace{[\tau_N-F_\partial(r)e_\epsilon]}_{(4)}d\mathtt{S} + \int_{t_1}^{t_2}\Big[\int_{\partial\Omega_D}\delta\tau_D^\top\underbrace{(r-r_D)}_{(5)}d\mathtt{S}\Big]\,dt = 0.$$

So applying the fundamental lemma of variational calculus, each term (i) with $i=\{1,...,5\}$ is equal to zero. Then, the following Lagrangian model with Dirichlet and Neumann BC is obtained:

$$\forall\mathtt{X}\in\Omega:\quad \mathcal{M}\ddot{r} = -\mathcal{F}_{\mathtt{X}}(r)^* e_\epsilon + b + B_d\,u_d, \tag{A.1}$$

$$\epsilon = \epsilon(r), \tag{A.2}$$

$$e_\epsilon = \frac{\partial\Psi(\epsilon)}{\partial\epsilon}, \tag{A.3}$$

$$\forall\mathtt{S}\in\partial\Omega_N:\quad \tau_N = F_\partial(r)\,e_\epsilon, \tag{A.4}$$

$$\forall\mathtt{S}\in\partial\Omega_D:\quad r_D = r. \tag{A.5}$$

Noticing that the time derivative of (A.2) leads to $\dot{\epsilon} = \mathcal{F}_{\mathtt{X}}(r)\dot{r} = \mathcal{F}_{\mathtt{X}}(r)e_p$, the Lagrangian model with Hamiltonian in (37) can be written as the explicit PHS in (33). The power exchange with the environment is given by:

$$\dot{H}(x) = \int_{\Omega} \delta_x H^\top \dot{x}\, d\mathtt{X} = \int_{\Omega} e_p^\top B_d\, u_d\, d\mathtt{X} + \underbrace{\int_{\Omega} (e_\epsilon^\top \mathcal{F}_{\mathtt{X}}(r) e_p - e_p^\top \mathcal{F}_{\mathtt{X}}(r)^* e_\epsilon) d\mathtt{X}}_{\text{Lemma 1}},$$

so applying Lemma 1 to the term indicated above we obtain:

$$\dot{H}(x) = \int_{\Omega} u_d^\top \underbrace{B_d^\top e_p}_{y_d}\, d\mathtt{X} + \int_{\partial\Omega} e_p^\top F_\partial(r) e_\epsilon\, d\mathtt{S} = \int_{\Omega} u_d^\top y_d\, d\mathtt{X} + \int_{\partial\Omega} u_\partial^\top y_\partial\, d\mathtt{S},$$

where u_∂ and y_∂ are the boundary inputs and outputs ports defined in (34). □

Proof of Proposition 4. From Step 4 in the proof of Theorem 1, note that each term (i) with $i = \{1, ..., 5\}$ is multiplied by a virtual displacement, virtual strain, virtual stress or virtual traction, and these products define virtual work. In addition, from (35) we get $\delta\tau_D(\mathtt{S}, t) = F_\partial(r)\delta e_\epsilon(\mathtt{S}, t)$, where there is no contribution of δr since it vanishes on $\partial\Omega_D$. Gathering the terms (1) and (4) and multiplying them by $\delta\dot{r}$, we get the virtual power expression in (39). Similarly, gathering the time derivative of the terms (2) and (5) and multiplying them by δe_ϵ and $\delta\tau_D$, respectively, we get the virtual power expression in (40). Lastly, multiplying the term (3) by $\delta\dot{\epsilon}$, we get the virtual power expression in (41). □

Proof of Theorem 2. For simplicity the spatial and temporal dependencies are omitted. From δP_p in (39) and the integration Lemma 1 we have:

$$\int_{\Omega} \delta\dot{\tilde{r}}^\top \mathcal{F}_{\mathtt{X}}(\tilde{r})^* \tilde{e}_\epsilon\, d\mathtt{X} = \int_{\Omega} \tilde{e}_\epsilon^\top \mathcal{F}_{\mathtt{X}}(\tilde{r})\, \delta\dot{\tilde{r}}\, d\mathtt{X} - \left(\int_{\partial\Omega_D} \delta\dot{\tilde{r}}^\top F_\partial(\tilde{r})\, \tilde{e}_\epsilon\, d\mathtt{S} + \int_{\partial\Omega_N} \delta\dot{\tilde{r}}^\top F_\partial(\tilde{r})\, \tilde{e}_\epsilon\, d\mathtt{S} \right),$$

where replacing in (39) we obtain:

$$\begin{aligned} \delta P_p = \quad & \delta\dot{\hat{r}}^\top \Bigg[\underbrace{\int_{\Omega} N_r^\top \mathcal{M} N_r\, d\mathtt{X}}_{\hat{M}}\, \ddot{\hat{r}} - \underbrace{\int_{\Omega} N_r^\top B_d N_{u_d} d\mathtt{X}}_{\hat{B}_d}\, \hat{u}_d - \underbrace{\int_{\Omega} N_r^\top b\, d\mathtt{X}}_{\hat{b}} - \underbrace{\int_{\partial\Omega_N} N_r^\top N_{\tau_N} d\mathtt{S}}_{\hat{B}_{\tau_N}}\, \hat{\tau}_N + ... \\ & ... \underbrace{\left(\int_{\Omega} (\mathcal{F}_{\mathtt{X}}(\tilde{r}) N_r)^\top N_e\, d\mathtt{X} - \int_{\partial\Omega_D} N_r^\top F_\partial(\tilde{r})\, N_e d\mathtt{S} \right)}_{\hat{\Sigma}(\hat{r})^\top} \hat{e} \Bigg] = 0. \end{aligned}$$

Using $\hat{p} = \hat{M}\dot{\hat{r}}$, the above equation leads to:

$$\dot{\hat{p}} = -\hat{\Sigma}(\hat{r})^\top \hat{e} + \hat{b} + \hat{B}_d\, \hat{u}_d + \hat{B}_{\tau_N} \hat{\tau}_N. \tag{A.6}$$

From δP_e in (40) we have:

$$\delta P_e = \delta\hat{e}^\top \Bigg[\underbrace{\int_{\Omega} N_e^\top N_\epsilon\, d\mathtt{X}}_{\hat{M}_e}\, \dot{\hat{\epsilon}} - \underbrace{\left(\int_{\Omega} N_e^\top \mathcal{F}_{\mathtt{X}}(\tilde{r}) N_r\, d\mathtt{X} - \int_{\partial\Omega_D} N_e^\top F_\partial(\tilde{r})^\top N_r\, d\mathtt{S} \right)}_{\hat{\Sigma}(\hat{r})} \dot{\hat{r}} - \underbrace{\int_{\partial\Omega_D} N_e^\top F_\partial(\tilde{r})^\top N_{v_D}\, d\mathtt{S}}_{\hat{\Gamma}(\hat{r})}\, \hat{v}_D \Bigg] = 0,$$

which using $\dot{\hat{r}} = \hat{M}^{-1}\hat{p} = \hat{e}_p$, $\hat{F}_x(\hat{r}) = \hat{M}_e^{-1}\hat{\Sigma}(\hat{r})$, and $\hat{B}_D(\hat{r}) = \hat{M}_e^{-1}\hat{\Gamma}(\hat{r})$ leads to:

$$\dot{\hat{\epsilon}} = \hat{F}_x(\hat{r})\hat{e}_p + \hat{B}_D(\hat{r})\hat{v}_D, \tag{A.7}$$

where $\hat{M}_e$ is invertible since $N_e(\mathtt{X}) = N_\epsilon(\mathtt{X})$. From δP_ϵ in (41) we have:

$$\delta P_\epsilon = \quad \delta\dot{\hat{\epsilon}}^\top \Bigg[\underbrace{\int_\Omega N_\epsilon^\top N_e \, d\mathtt{X}}_{\hat{M}_e^\top} \hat{e} - \underbrace{\int_\Omega N_\epsilon^\top \frac{\partial \Psi}{\partial \epsilon}\Big|_{\epsilon=\tilde{\epsilon}} d\mathtt{X}}_{\hat{e}_\epsilon(\hat{\epsilon})} \Bigg] = 0,$$

which leads to:

$$\hat{e} = \hat{M}_e^{-\top} \hat{e}_\epsilon(\hat{\epsilon}). \tag{A.8}$$

Replacing (A.8) into (A.6), together with (A.7) and $\dot{\hat{r}} = \hat{e}_p$, they define the discretized finite-dimensional PHS in (43). Regarding the elastic potential energy, it is trivial that $\hat{U}(\hat{\epsilon}) = \int_\Omega \Psi(\tilde{\epsilon}) \, d\mathtt{X} = \int_\Omega \Psi(N_e \, \hat{\epsilon}) \, d\mathtt{X}$. Lastly:

$$\nabla_{\hat{\epsilon}} \hat{U}(\hat{\epsilon}) = \frac{\partial}{\partial \hat{\epsilon}} \int_\Omega \Psi(N_\epsilon \, \hat{\epsilon}) \, d\mathtt{X} = \int_\Omega N_\epsilon^\top \frac{\partial \Psi}{\partial \epsilon}\Big|_{\epsilon \, = \, \tilde{\epsilon}} d\mathtt{X} = \hat{e}_\epsilon(\hat{\epsilon}),$$

which concludes the proof. □

***Proof of Proposition** 5.* For simplicity the spatial and temporal dependencies are omitted. From Step 4 in the proof of Theorem 1, we gather terms (2) and (5) and multiply them by δe_ϵ and $\delta \tau_D = F_\partial(r) \delta e_\epsilon$, respectively. This leads to the virtual work expression in (61). Using the approximations introduced in (42), along with $\tilde{r}_D(\mathtt{S}, t) = N_{v_D}(\mathtt{S}) \, \hat{r}_D(t)$, and substituting into (61) we obtain:

$$\delta\hat{e}^\top \Bigg[\underbrace{\int_\Omega N_e^\top N_\epsilon \, d\mathtt{X}}_{\hat{M}_e} \hat{\epsilon} - \underbrace{\int_\Omega N_e^\top \epsilon(\tilde{r}) N_r \, d\mathtt{X}}_{\hat{\Phi}(\hat{r})} + \underbrace{\int_{\partial\Omega_D} N_e^\top F_\partial(\tilde{r})^\top N_r \, d\mathtt{S}}_{\hat{\Upsilon}(\hat{r})} \hat{r} - \underbrace{\int_{\partial\Omega_D} N_e^\top F_\partial(\tilde{r})^\top N_{v_D} \, d\mathtt{S}}_{\hat{\Gamma}(\hat{r})} \hat{r}_D \Bigg] = 0,$$

from which we obtain: $\hat{\epsilon} = \underbrace{\hat{M}_e^{-1}(\hat{\Phi}(\hat{r}) - \hat{\Upsilon}(\hat{r})\hat{r})}_{\hat{\epsilon}(\hat{r})} + \underbrace{\hat{M}_e^{-1}\hat{\Gamma}(\hat{r})}_{\hat{B}_D(\hat{r})} \hat{r}_D$, which matches (62) and concludes the proof.

□

Appendix B. Numerical time integration schemes

One of the main challenges in the time integration of discretized nonlinear FEM-based models lies in the evaluation, spatial integration, and assembly of nonlinear terms at each time step, such as $\hat{F}_x(\hat{r})$, $\hat{B}_D(\hat{r})$, and $\hat{e}_\epsilon(\hat{\epsilon})$, due to their high computational cost. This issue is further compounded when using implicit time integration schemes, which require solving a nonlinear system of equations at each step, typically via iterative methods. Explicit methods have the advantage of avoiding such nonlinear solvers at each time step, significantly reducing computational cost by requiring only the evaluation of nonlinear terms. However, their stability is limited by the time step size, and they may fail to accurately capture the system's energy behavior. In contrast, implicit methods such as the implicit midpoint rule provide greater stability for larger time steps and improved energy behavior, albeit at a higher computational cost due to the nonlinear solves.

To address these challenges, this work adopts two simulation strategies. The first is an explicit scheme inspired by the Störmer–Verlet method, originally developed for Hamiltonian systems with two variables: momentum and displacement. Since our PHS models include an additional strain variable, the method is extended to accommodate this structure. The second approach applies the implicit midpoint rule, supplemented with a predictor step based on the Störmer–Verlet scheme. This predictor provides an initial guess for the iterative nonlinear solver, aimed to reduce the number of iterations per time step and, consequently, the overall computational cost.

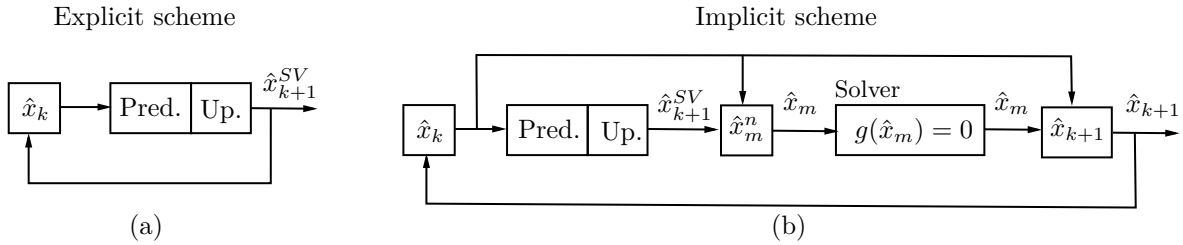

Figure B.1: (a) Extended Störmer–Verlet. (b) Implicit midpoint rule with Störmer–Verlet as predictor.

Appendix B.1. Explicit scheme

Before presenting the extension of the Störmer–Verlet method, we first introduce the classical method applied to a Hamiltonian system:

$$\begin{bmatrix}\dot{p}(t)\\ \dot{r}(t)\end{bmatrix} = \begin{bmatrix}0 & -I\\ I & 0\end{bmatrix}\begin{bmatrix}\nabla_p H(p,r)\\ \nabla_r H(p,r)\end{bmatrix} + \begin{bmatrix}I\\ 0\end{bmatrix} u(t). \tag{B.1}$$

The Störmer–Verlet method consists of a prediction step given by:

$$\frac{p_{k+1/2} - p_k}{\Delta t/2} = -\nabla_r H(p_{k+1/2}, r_k) + u(t_k), \tag{B.2}$$

$$\frac{r_{k+1} - r_k}{\Delta t} = \nabla_p H(p_{k+1/2}, r_{k+1}), \tag{B.3}$$

where Δt is the time step, (B.2) is implicit in $p_{k+1/2}$ and must be solved for this variable, while equation (B.3) is implicit in r_{k+1} and must be solved accordingly [64]. Next, the update step is performed as:

$$\frac{p_{k+1} - p_{k+1/2}}{\Delta t/2} = -\nabla_r H(p_{k+1/2}, r_{k+1}) + u(t_{k+1/2}), \tag{B.4}$$

where $t_{k+1/2} = t_k + \Delta t/2$ is the midpoint time, and (B.4) is implicit in p_{k+1}.

Method 1 (Explicit scheme). The explicit extended Störmer–Verlet scheme for time integration of the nonlinear PHS in (43) is given by:

Prediction step:

$$\hat{p}_{k+1/2} = \hat{p}_k + \frac{\Delta t}{2}\left[-\hat{F}_x(\hat{r}_k)^\top \hat{e}_\epsilon(\hat{\epsilon}_k) + \hat{b} + \hat{B}_d \hat{u}_d(t_k) + \hat{B}_N \hat{\tau}_N(t_k)\right],$$

$$\hat{\epsilon}_{k+1/2} = \hat{\epsilon}_k + \frac{\Delta t}{2}\left[\hat{F}_x(\hat{r}_k)\hat{M}^{-1}\hat{p}_{k+1/2} + \hat{B}_D(\hat{r}_k)\hat{v}_D(t_k)\right],$$

$$\hat{r}_{k+1} = \hat{r}_k + \frac{\Delta t}{2}\hat{M}^{-1}\hat{p}_{k+1/2}.$$

Update step:

$$\hat{p}_{k+1} = \hat{p}_{k+1/2} + \frac{\Delta t}{2}\left[-\hat{F}_x(\hat{r}_{k+1})^\top \hat{e}_\epsilon(\hat{\epsilon}_{k+1/2}) + \hat{b} + \hat{B}_d \hat{u}_d(t_{k+1/2}) + \hat{B}_N \hat{\tau}_N(t_{k+1/2})\right],$$

$$\hat{\epsilon}_{k+1} = \hat{\epsilon}_{k+1/2} + \frac{\Delta t}{2}\left[\hat{F}_x(\hat{r}_{k+1})\hat{M}^{-1}\hat{p}_{k+1} + \hat{B}_D(\hat{r}_{k+1})\hat{v}_D(t_{k+1/2})\right],$$

The next state is denoted as: $\hat{x}^{SV}_{k+1} = \begin{bmatrix}\hat{p}_{k+1}\\ \hat{\epsilon}_{k+1}\\ \hat{r}_{k+1}\end{bmatrix}$.

Appendix B.2. Implicit scheme

Consider a nonlinear dynamical system of the form: $\dot{x} = f(x,t)$. The application of the implicit midpoint rule to this system yields:

$$g(x_m) = x_m - x_k - \frac{\Delta t}{2} f(x_m, t_{k+1/2}) = 0, \tag{B.5}$$

where $x_m = (x_{k+1} + x_k)/2$ denotes the midpoint state. At each time step, solving $g(x_m) = 0$ for x_m is required, typically using iterative methods. For instance, the Newton–Raphson method updates the initial guess x_m^n as:

$$x_m^{n+1} = x_m^n - J_g(x_m^n)^{-1} g(x_m^n), \tag{B.6}$$

where the Jacobian matrix $J_g(x_m)$ is given by:

$$J_g(x_m) = \frac{\partial g}{\partial x_m} = I - \frac{\Delta t}{2} \frac{\partial f}{\partial x_m}. \tag{B.7}$$

Convergence is achieved when a prescribed criterion is met, for instance: $\|g(x_m^n)\| < \text{tol}$. A better initial guess x_m^n typically leads to a faster convergence of the nonlinear solver. Once x_m is computed, the next state is obtained as $x_{k+1} = 2x_m - x_k$.

Method 2 (Implicit scheme). The implicit midpoint rule applied to the finite-dimensional nonlinear PHS in (43), using the extended Störmer–Verlet scheme in Method 1 as predictor for the midpoint state $\hat{x}_m$, is summarized as follows:

1. Estimate $\hat{x}_{k+1}^{SV}$ using Method 1.
2. Compute the initial guess: $\hat{x}_m^n = \dfrac{\hat{x}_{k+1}^{SV} + \hat{x}_k}{2}$.
3. Solve for $\hat{x}_m$: $\quad g(\hat{x}_m) = \hat{x}_m - \hat{x}_k - \dfrac{\Delta t}{2} \hat{J}(\hat{x}_m) \nabla_{\hat{x}} \hat{H}(\hat{x}_m) - \dfrac{\Delta t}{2} \hat{G}(\hat{x}_m) \hat{u}(t_{k+1/2}) = 0.$
4. Compute the next state: $\hat{x}_{k+1} = 2\hat{x}_m - \hat{x}_k$.

Neither the extended Störmer–Verlet method nor the implicit midpoint rule guarantees exact energy preservation in nonlinear systems. However, the implicit midpoint rule is expected to yield better energy behavior due to its symplectic structure and fully implicit formulation. A rigorous analysis of energy conservation, convergence, and error properties of the implemented time integrators is beyond the scope of this work.

References

[1] M. Bhatti, M. Marin, R. Ellahi, I. Fudulu, Insight into the dynamics of EMHD hybrid nanofluid (ZnO/CuO-SA) flow through a pipe for geothermal energy applications, Journal of Thermal Analysis and Calorimetry 148 (24) (2023) 14261–14273.
[2] Z. Shi, L. Li, T. He, Thermoelastic transient memory response analysis of non-localized nano-piezoelectric plates based on Moore-Gibson-Thompson thermoelasticity theory, The Journal of Strain Analysis for Engineering Design 59 (3) (2024) 194–206.
[3] B. Rende, I. F. Santos, Theoretical contribution to multiphysical modeling of flywheel energy storage systems with a focus on thermal effects in magnetic bearings, Journal of Energy Storage 130 (2025) 117276.
[4] J. Childs, C. Rucker, Leveraging geometry to enable high-strength continuum robots, Frontiers in Robotics and AI 8 (2021) 629871.
[5] T. Li, C. Keplinger, R. Baumgartner, S. Bauer, W. Yang, Z. Suo, Giant voltage-induced deformation in dielectric elastomers near the verge of snap-through instability, Journal of the Mechanics and Physics of Solids 61 (2) (2013) 611–628.
[6] Y. Liu, K. Luo, Q. Tian, H. Hu, Nonlinear dynamics design for in-space assembly motion of manipulators on flexible base structures, Nonlinear Dynamics (2025) 1–23.
[7] G. Rega, Nonlinear dynamics in mechanics: state of the art and expected future developments, Journal of Computational and Nonlinear Dynamics 17 (8) (2022) 080802.

[8] E. Bayo, J. G. De Jalon, M. A. Serna, A modified Lagrangian formulation for the dynamic analysis of constrained mechanical systems, Computer methods in applied mechanics and engineering 71 (2) (1988) 183–195.
[9] Z. Yosibash, R. Kirby, Dynamic response of various von-Kármán non-linear plate models and their 3-D counterparts, International journal of solids and structures 42 (9-10) (2005) 2517–2531.
[10] Y. Yu, P. Qi, K. Althoefer, H.-K. Lam, Lagrangian dynamics and nonlinear control of a continuum manipulator, in: 2015 IEEE International Conference on Robotics and Biomimetics (ROBIO), IEEE, 2015, pp. 1912–1917.
[11] T. Belytschko, W. Liu, B. Moran, K. Elkhodary, Nonlinear finite elements for continua and structures, John wiley & sons, 2014.
[12] J. Hales, S. Novascone, R. Williamson, D. Gaston, M. Tonks, Solving nonlinear solid mechanics problems with the Jacobian-free Newton Krylov method, Computer Modeling in Engineering and Sciences 84 (2) (2012) 123.
[13] N. Saeed, S. Abdulkarim, A review of nonlinear control strategies for shape and stress in structural engineering, in: P. Y. Chen, V. Martinez-Luaces (Eds.), Nonlinear Systems and Matrix Analysis, IntechOpen, Rijeka, 2024, Ch. 2. doi:10.5772/intechopen.1004811.
URL https://doi.org/10.5772/intechopen.1004811
[14] A. van der Schaft, B. Maschke, Hamiltonian formulation of distributed-parameter systems with boundary energy flow, Journal of Geometry and physics 42 (1-2) (2002) 166–194.
[15] B. Maschke, A. van der Schaft, Port-controlled Hamiltonian systems: modelling origins and systemtheoretic properties, in: Nonlinear Control Systems Design 1992, Elsevier, 1993, pp. 359–365.
[16] V. Duindam, A. Macchelli, S. Stramigioli, H. Bruyninckx, Modeling and control of complex physical systems: the port-Hamiltonian approach, Springer Science & Business Media, 2009.
[17] R. Rashad, S. Stramigioli, The port-Hamiltonian structure of continuum mechanics, Journal of Nonlinear Science 35 (2) (2025) 35.
[18] F. Califano, R. Rashad, F. Schuller, S. Stramigioli, Energetic decomposition of distributed systems with moving material domains: The port-Hamiltonian model of fluid-structure interaction, Journal of geometry and physics 175 (2022) 104477.
[19] N. Javanmardi, P. Borja, A. van der Schaft, M. Yazdanpanah, J. Scherpen, Energy-based trajectory tracking for underactuated mechanical systems: Velocity-free and disturbance rejection methods, Authorea Preprint.
[20] R. Ortega, A. van der Schaft, F. Castanos, A. Astolfi, Control by interconnection and standard passivity-based control of port-Hamiltonian systems, IEEE Transactions on Automatic control 53 (11) (2008) 2527–2542.
[21] H. Ramirez, H. Zwart, Y. Le Gorrec, Stabilization of infinite dimensional port-Hamiltonian systems by nonlinear dynamic boundary control, Automatica 85 (2017) 61–69.
[22] J. Schmid, H. Zwart, Stabilization of port-Hamiltonian systems by nonlinear boundary control in the presence of disturbances, ESAIM: Control, Optimisation and Calculus of Variations 27 (2021) 53.
[23] F. Cardoso-Ribeiro, G. Haine, Y. Le Gorrec, D. Matignon, H. Ramirez, Port-Hamiltonian formulations for the modeling, simulation and control of fluids, Computers & Fluids (2024) 106407.
[24] R. Rashad, F. Califano, A. van der Schaft, S. Stramigioli, Twenty years of distributed port-Hamiltonian systems: a literature review, IMA Journal of Mathematical Control and Information 37 (4) (2020) 1400–1422.
[25] A. Brugnoli, R. Rashad, F. Califano, S. Stramigioli, D. Matignon, Mixed finite elements for port-Hamiltonian models of von Kármán beams, IFAC-papersonline 54 (19) (2021) 186–191.
[26] T. Voss, J. Scherpen, P. Onck, Modeling for control of an inflatable space reflector, the nonlinear 1-D case, in: 2008 47th IEEE Conference on Decision and Control, IEEE, 2008, pp. 1777–1782.
[27] T. Voss, J. Scherpen, Port-Hamiltonian modeling of a nonlinear Timoshenko beam with piezo actuation, SIAM Journal on Control and Optimization 52 (1) (2014) 493–519.
[28] M. Trivedi, R. Banavar, P. Kotyczka, Hamiltonian modelling and buckling analysis of a nonlinear flexible beam with actuation at the bottom, Mathematical and Computer Modelling of Dynamical Systems 22 (5) (2016) 475–492.
[29] A. Brugnoli, D. Matignon, A port-Hamiltonian formulation for the full von-Kármán plate model, in: 10th European Nonlinear Dynamics Conference (ENOC), 2022, p. 0.
[30] T. Thoma, P. Kotyczka, H. Egger, On the velocity-stress formulation for geometrically nonlinear elastodynamics and its structure-preserving discretization, Mathematical and Computer Modelling of Dynamical Systems 30 (1) (2024) 701–720.
[31] P. Kinon, P. Betsch, S. Eugster, Energy-momentum-consistent simulation of planar geometrically exact beams in a port-Hamiltonian framework, Multibody System Dynamics (2025) 1–33.
[32] P. Kinon, T. Thoma, P. Betsch, P. Kotyczka, Port-Hamiltonian formulation and structure-preserving discretization of hyperelastic strings, arXiv preprint arXiv:2304.10957.
[33] C. Ponce, Y. Wu, Y. Le Gorrec, H. Ramirez, Port-Hamiltonian modeling of a geometrically nonlinear hyperelastic beam, IFAC-PapersOnLine 58 (6) (2024) 309–314.
[34] M. Seslija, A. van der Schaft, J. Scherpen, Discrete exterior geometry approach to structure-preserving discretization of distributed-parameter port-Hamiltonian systems, Journal of Geometry and Physics 62 (6) (2012) 1509–1531.
[35] A. Brugnoli, R. Rashad, S. Stramigioli, Dual field structure-preserving discretization of port-Hamiltonian systems using finite element exterior calculus, Journal of computational physics 471 (2022) 111601.
[36] G. Golo, V. Talasila, A. van der Schaft, B. Maschke, Hamiltonian discretization of boundary control systems, Automatica 40 (5) (2004) 757–771.
[37] P. Kotyczka, Finite volume structure-preserving discretization of 1D distributed-parameter port-Hamiltonian systems, IFAC-PapersOnLine 49 (8) (2016) 298–303.
[38] A. Serhani, D. Matignon, G. Haine, Structure-preserving finite volume method for 2D linear and non-linear port-Hamiltonian systems, IFAC-PapersOnLine 51 (3) (2018) 131–136.
[39] T. Thoma, P. Kotyczka, Explicit port-Hamiltonian FEM-models for linear mechanical systems with non-uniform boundary

conditions, IFAC-PapersOnLine 55 (20) (2022) 499–504.
[40] V. Trenchant, H. Ramirez, Y. Le Gorrec, P. Kotyczka, Finite differences on staggered grids preserving the port-Hamiltonian structure with application to an acoustic duct, Journal of Computational Physics 373 (2018) 673–697.
[41] P. Bochev, J. Hyman, Principles of mimetic discretizations of differential operators, in: Compatible spatial discretizations, Springer, 2006, pp. 89–119.
[42] Y. Yu, Generalized Hamilton's principle and variational equation of motion in nonlinear elasticity theory, with application to plate theory, The Journal of the Acoustical Society of America 36 (1) (1964) 111–120.
[43] Y. Le Gorrec, H. Zwart, B. Maschke, A semigroup approach to port-Hamiltonian systems associated with linear skew symmetric operator, in: 16th international symposium on mathematical theory of networks and systems (MTNS 2004), 2004.
[44] Y. Le Gorrec, H. Zwart, B. Maschke, Dirac structures and boundary control systems associated with skew-symmetric differential operators, SIAM journal on control and optimization 44 (5) (2005) 1864–1892.
[45] A. Brugnoli, A port-Hamiltonian formulation of flexible structures. Modelling and structure-preserving finite element discretization, Ph.D. thesis, ISAE-Institut Supérieur de l'Aéronautique et de l'Espace (2020).
[46] A. Macchelli, A. van der Schaft, C. Melchiorri, Port-Hamiltonian formulation of infinite dimensional systems I. Modeling, in: 2004 43rd IEEE Conference on Decision and Control (CDC)(IEEE Cat. No. 04CH37601), Vol. 4, IEEE, 2004, pp. 3762–3767.
[47] G. Nishida, M. Yamakita, Formal distributed port-Hamiltonian representation of field equations, in: Proceedings of the 44th IEEE Conference on Decision and Control, IEEE, 2005, pp. 6009–6015.
[48] G. Nishida, M. Yamakita, Z.-w. Luo, Field port-Lagrangian representation of conservation laws for variational symmetries, in: Proceedings of the 45th IEEE Conference on Decision and Control, IEEE, 2006, pp. 5875–5881.
[49] M. Schöberl, A. Siuka, Jet bundle formulation of infinite-dimensional port-Hamiltonian systems using differential operators, Automatica 50 (2) (2014) 607–613.
[50] M. Schöberl, A. Siuka, Analysis and comparison of port-Hamiltonian formulations for field theories-demonstrated by means of the Mindlin plate, in: 2013 European Control Conference (ECC), IEEE, 2013, pp. 548–553.
[51] C. Ponce, Y. Wu, Y. Le Gorrec, H. Ramirez, A systematic methodology for port-hamiltonian modeling of multidimensional flexible linear mechanical systems, Applied Mathematical Modelling 134 (2024) 434–451.
[52] C. Ponce, Port-hamiltonian modeling, discretization and shape control of multidimensional flexible mechanical systems, Ph.D. thesis, Université Bourgogne Franche-Comté; Universidad técnica Federico Santa María (2024).
[53] T. Beda, Modeling hyperelastic behavior of rubber: A novel invariant-based and a review of constitutive models, Journal of Polymer Science Part B: Polymer Physics 45 (13) (2007) 1713–1732.
[54] G. Chagnon, M. Rebouah, D. Favier, Hyperelastic energy densities for soft biological tissues: a review, Journal of Elasticity 120 (2015) 129–160.
[55] S. Melly, L. Liu, Y. Liu, J. Leng, A review on material models for isotropic hyperelasticity, International Journal of Mechanical System Dynamics 1 (1) (2021) 71–88.
[56] H. Khaniki, M. Ghayesh, R. Chin, M. Amabili, A review on the nonlinear dynamics of hyperelastic structures, Nonlinear Dynamics 110 (2) (2022) 963–994.
[57] J. Reddy, An Introduction to Nonlinear Finite Element Analysis Second Edition: with applications to heat transfer, fluid mechanics, and solid mechanics, OUP Oxford, 2014.
[58] J. T. Oden, Finite elements of nonlinear continua, Courier Corporation, 2006.
[59] R. Ogden, Non-linear elastic deformations, Courier Corporation, 1997.
[60] P. Wriggers, Mixed finite element methods-theory and discretization, in: Mixed finite element technologies, Springer, 2009, pp. 131–177.
[61] J. C. Simo, M. Rifai, A class of mixed assumed strain methods and the method of incompatible modes, International journal for numerical methods in engineering 29 (8) (1990) 1595–1638.
[62] J. C. Simo, F. Armero, Geometrically non-linear enhanced strain mixed methods and the method of incompatible modes, International journal for numerical methods in engineering 33 (7) (1992) 1413–1449.
[63] J. Reddy, Theory and analysis of elastic plates and shells, CRC press, 2006.
[64] E. Hairer, C. Lubich, G. Wanner, Geometric numerical integration illustrated by the Störmer–Verlet method, Acta numerica 12 (2003) 399–450.
[65] A. Brugnoli, D. Matignon, J. Morlier, Exact energy-conserving and linear discretization scheme for geometrically non-linear models, in: 16ème Colloque National en Calcul de Structures, 2024.
[66] A. Brugnoli, D. Matignon, J. Morlier, A linearly-implicit energy preserving scheme for geometrically nonlinear mechanics based on non-canonical Hamiltonian formulations, arXiv preprint arXiv:2503.04695.
[67] P. Kinon, R. Morandin, P. Schulze, Discrete gradient methods for port-Hamiltonian differential-algebraic equations, arXiv preprint arXiv:2505.18810.
[68] P. Kinon, T. Thoma, P. Betsch, P. Kotyczka, Generalized Maxwell viscoelasticity for geometrically exact strings: Nonlinear port-Hamiltonian formulation and structure-preserving discretization, IFAC-PapersOnLine 58 (6) (2024) 101–106.
[69] M. Hille, M. Franke, F. Zähringer, P. Betsch, Structure-preserving discretization of a polyconvexity-inspired formulation for coupled nonlinear electro-thermo-elastodynamics, IFAC-PapersOnLine 58 (6) (2024) 113–118.
[70] P. Pedersen, Analytical stiffness matrices for tetrahedral elements, Computer methods in applied mechanics and engineering 196 (1-3) (2006) 261–278.
[71] E. Gülümser, U. Güdükbay, S. Filiz, Fast stiffness matrix calculation for nonlinear finite element method, Journal of Applied Mathematics 2014 (1) (2014) 932314.